

Exactly Sparse Gaussian Variational Inference with Application to Derivative-Free Batch Nonlinear State Estimation

©The Author(s) 2020

Timothy D. Barfoot¹ and James R. Forbes² and David J. Yoon¹

Abstract

We present a Gaussian Variational Inference (GVI) technique that can be applied to large-scale nonlinear batch state estimation problems. The main contribution is to show how to fit both the mean and (inverse) covariance of a Gaussian to the posterior efficiently, by exploiting factorization of the joint likelihood of the state and data, as is common in practical problems. This is different than Maximum A Posteriori (MAP) estimation, which seeks the point estimate for the state that maximizes the posterior (i.e., the mode). The proposed Exactly Sparse Gaussian Variational Inference (ESGVI) technique stores the inverse covariance matrix, which is typically very sparse (e.g., block-tridiagonal for classic state estimation). We show that the only blocks of the (dense) covariance matrix that are required during the calculations correspond to the non-zero blocks of the inverse covariance matrix, and further show how to calculate these blocks efficiently in the general GVI problem. ESGVI operates iteratively, and while we can use analytical derivatives at each iteration, Gaussian cubature can be substituted, thereby producing an efficient derivative-free batch formulation. ESGVI simplifies to precisely the Rauch-Tung-Striebel (RTS) smoother in the batch linear estimation case, but goes beyond the ‘extended’ RTS smoother in the nonlinear case since it finds the best-fit Gaussian (mean and covariance), not the MAP point estimate. We demonstrate the technique on controlled simulation problems and a batch nonlinear Simultaneous Localization and Mapping (SLAM) problem with an experimental dataset.

Keywords

Gaussian variational inference, exact sparsity, derivative-free state estimation

1 Introduction

Gauss pioneered the method of least squares out of necessity to predict the position of the dwarf planet Ceres after passing behind the Sun. In his initial treatment of the subject (Gauss 1809), he presented what we would consider a ‘likelihood’ function, which was expressed as an exponential function of quadratic terms,

$$L(\mathbf{x}) = \exp\left(-\frac{1}{2}(\mathbf{x} - \mathbf{z})^T \mathbf{W}^{-1}(\mathbf{x} - \mathbf{z})\right), \quad (1)$$

where \mathbf{x} is the state to be estimated, \mathbf{z} are measurements, and \mathbf{W}^{-1} is a weighting matrix. Gauss recognized that $L(\mathbf{x})$ is maximized when $(\mathbf{x} - \mathbf{z})^T \mathbf{W}^{-1}(\mathbf{x} - \mathbf{z})$ is minimized, leading to the weighted least-squares solution. He later proved that the least-squares estimate is optimal without any assumptions regarding the distribution errors (Gauss 1821, 1823), and his more general result was rediscovered by Markoff (1912), leading to the more commonly known Gauss-Markov theorem (Bjorck 1996).

If we adopt a Bayesian perspective (Bayes 1764), our goal is to compute the full posterior, $p(\mathbf{x}|\mathbf{z})$, by refining a prior, $p(\mathbf{x})$, not just a point estimate, based on some measurements, \mathbf{z} :

$$p(\mathbf{x}|\mathbf{z}) = \frac{p(\mathbf{z}|\mathbf{x})p(\mathbf{x})}{p(\mathbf{z})} = \frac{p(\mathbf{x}, \mathbf{z})}{p(\mathbf{z})}. \quad (2)$$

The full posterior is not a Gaussian Probability Density Function (PDF) for nonlinear measurement models, $p(\mathbf{z}|\mathbf{x})$. We are therefore often satisfied with finding the maximum of the Bayesian posterior, which is called the Maximum

¹Institute for Aerospace Studies, University of Toronto

²Department of Mechanical Engineering, McGill University

Corresponding author:

Timothy D. Barfoot, Institute for Aerospace Studies, University of Toronto, Toronto, Ontario, M3H 5T6, Canada.

Email: tim.barfoot@utoronto.ca

A Posteriori (MAP) approach. The connection to least squares (for Gaussian noise) is seen by taking the negative logarithm of the likelihood function (and dropping constant terms), resulting in a nonlinear quadratic loss function that is minimized:

$$\begin{aligned} V(\mathbf{x}) &= -\ln p(\mathbf{x}, \mathbf{z}) = \frac{1}{2} \mathbf{e}(\mathbf{x}, \mathbf{z})^T \mathbf{W}^{-1} \mathbf{e}(\mathbf{x}, \mathbf{z}), \\ \mathbf{x}^* &= \arg \min_{\mathbf{x}} V(\mathbf{x}), \end{aligned} \quad (3)$$

where $\mathbf{e}(\cdot, \cdot)$ is the error and is a nonlinear function of the state, \mathbf{x} , and measurements, \mathbf{z} . The result is a *point solution*, the most likely \mathbf{x} given \mathbf{z} . A Bayesian prior can easily be included in the loss function and thus we refer to this problem as MAP rather than Maximum Likelihood (ML) (no prior). Although there are various methods for minimizing the above loss function, perhaps the most well known dates back, again, to Gauss, who described how nonlinear least-squares problems can be linearized and refined in an iterative process (Abdulle and Wanner 2002), a method that is now known as Gauss-Newton (GN), or the method of differential corrections (Ortega and Rheinboldt 1970). To this day, MAP is the dominant approach employed for batch nonlinear estimation problems.

Rather than finding the maximum of the Bayesian posterior, our approach in this paper will be to find the best Gaussian approximation, in terms of the mean and (inverse) covariance, to the full posterior that is ‘closest’ in terms of the Kullback-Leibler (KL) divergence between the two (Kullback and Leibler 1951). This approach is referred to as *variational inference* or *variational Bayes* (Bishop 2006). As we will restrict ourselves to Gaussian approximations of the posterior, we will refer to this as *Gaussian variational inference* (GVI). While GVI is not new, it is not commonly used in batch estimation problems, where the state size, N , can be very large. Our main contribution in this paper, is to show how to make GVI tractable for large-scale estimation problems. Specifically, we will show how to exploit a joint likelihood for the state and measurements that can be factored,

$$p(\mathbf{x}, \mathbf{z}) = \prod_{k=1}^K p(\mathbf{x}_k, \mathbf{z}_k), \quad (4)$$

where \mathbf{x}_k is a subset of the variables in \mathbf{x} . This type of factorization is very common in real-world robotics problems, for example, since each measurement typically only involves a small subset of the state variables and this is already exploited in the MAP approach (Brown 1958; Thrun et al. 2004; Walter et al. 2007) for efficient solutions. We extend this exploit to the GVI approach by identifying that the inverse covariance matrix is *exactly sparse* when the likelihood factors, and most importantly, that we never actually need to compute the entire covariance matrix, which is typically dense and of size $N \times N$.

As a by-product of our approach, we also show how to use cubature points (e.g., sigmapoints) for some of the required calculations, resulting in an efficient derivative-free implementation for large-scale batch estimation.

The paper is organized as follows. Section 2 reviews some related work. Section 3 sets up our GVI approach in terms of the KL functional that we seek to minimize. It then derives a Newton-style iterative optimizer to calculate the mean and (inverse) covariance of the Gaussian approximation. Section 4 shows how we can exploit a factored likelihood not only by showing the inverse covariance is exactly sparse (as it is in the MAP formulation) but also showing that we only ever require the blocks of the covariance matrix corresponding to the non-zero blocks of the inverse covariance. It also summarizes an existing method for calculating these required blocks of the covariance and shows how we can make use of sample-based methods to avoid the need to calculate derivatives of our models. Section 5 presents an alternate formulation of the variational approach that is more approximate but also more efficient and also shows how we can fold parameter estimation into the framework while still exploiting sparsity. Section 6 provides some toy problems and a real-data robotics demonstration of the method. Finally, Section 7 provides our conclusion and suggestions for future work.

2 Related Work

Gaussian estimation has been a key tool employed in fields such as robotics, computer vision, aerospace, and more. The famous Kalman Filter (KF) (Kalman 1960), for example, provides a recursive formula to propagate a Gaussian state estimate. While the KF only goes forward in time, the Rauch-Tung-Striebel (RTS) smoother (Rauch et al. 1965) carries out forward and backward passes to efficiently estimate the state and can be shown to be carrying out full Bayesian inference for linear models (Barfoot 2017). Särkkä (2013) provides a wonderful presentation of recursive Bayesian inference methods, for both linear and nonlinear models. In computer vision and robotics, the important Bundle Adjustment (BA) (Brown 1958) / Simultaneous Localization and Mapping (SLAM) (Durrant-Whyte and Bailey 2006) problem is often cast as a batch Gaussian estimation problem (Triggs et al. 2000; Lu and Milios 1997; Thrun and Montemerlo 2005), with more advanced solution methods required than simple forward/backward passes (Kaess et al. 2008, 2011).

While the recursive methods are fundamentally important, here we concern ourselves with problems that require batch Gaussian inference. In robotics, some canonical problems are batch trajectory estimation, pose-graph relaxation (Bourmaud 2016), and BA/SLAM. However, we can also pose control/planning (Dong et al. 2016; Mukadam

et al. 2018), calibration (Pradeep et al. 2014), and three-dimensional modelling problems (Li et al. 2011) as Gaussian inference, such that the number of commonplace applications is quite large. Despite the widespread need for this tool, almost without exception we rely on MAP estimation to ‘fit’ a Gaussian, which is to say we find the most likely state in the Bayesian posterior and call this the ‘mean’, then fit a Gaussian centered at the most likely state, which is referred to as the Laplace approximation (Bishop 2006, p. 315). For linear models, this in fact does produce the exact Gaussian posterior. For nonlinear models, however, the posterior is not Gaussian and then the Laplace approximation is a convenient approach that can be computed efficiently for large-scale problems. The primary goal of this paper is to revisit the batch Gaussian inference problem in search of improvements over this popular method.

Within recursive estimation, attempts have been made to go beyond MAP, in order to perform better on nonlinear problems. The Bayes filter (Jazwinski 1970) is a general method that can be approximated in many different ways including through the use of Monte Carlo integration (Thrun et al. 2006) or the use of cubature rules (e.g., sigmapoints) (Julier and Uhlmann 1996; Särkkä 2013). These sample-based extensions also bring the convenience of not requiring analytical derivatives of nonlinear models to be calculated. Thus, a secondary goal of the paper is to find principled ways of incorporating sample-based techniques within batch Gaussian inference.

As we will see, the starting point for our paper will be a variational Bayes setup (Bishop 2006). We aim to find the Gaussian approximation that is closest to the full Bayesian posterior in terms of the KL divergence between the two (Kullback and Leibler 1951). This is a paradigm shift from the MAP approach where the only parameter to be optimized is the ‘mean’, while the Laplace-style covariance is computed post hoc. In GVI, we seek to find the best mean and covariance from the outset. The challenge is how to do this efficiently for problems with a large state size; if the mean is size N , then the covariance will be $N \times N$, which for real-world problems could be prohibitively expensive. However, as we will show, we can carry out full GVI by exploiting the same problem structures we usually do in the MAP approach. This will come at the expense of some increased computational cost, but the computational complexity as a function of N does not increase. Ranganathan et al. (2007) and recently Davison and Ortiz (2019) discuss the use of loopy belief propagation to carry out large-scale Gaussian inference for robotics problems; our motivation is somewhat different in that we seek to improve on MAP whereas these works investigate parallelization of the computations and further approximate the Gaussian variational estimate.

While this result is new in robotics, Oppner and Archambeau (2009) discuss a similar GVI approach in machine learning. They begin with the same KL divergence and show how to calculate the derivatives of this functional with respect to the Gaussian parameters. They go on to apply the method to Gaussian process regression problems (Rasmussen and Williams 2006), of which batch trajectory estimation can be viewed as a special case (Barfoot et al. 2014; Anderson et al. 2015). Our paper extends this work in several significant ways including (i) generalizing to any GVI problem where the likelihood can be factored, (ii) devising a Newton-style iterative solver for both mean and inverse covariance, (iii) explicitly showing how to exploit problem-specific structure in the case of a factored likelihood to make the technique efficient, (iv) applying Gaussian cubature to avoid the need to calculate derivatives, and (v) demonstrating the approach on problems of interest in robotics.

Kokkala et al. (2014, 2016), Ala-Luhtala et al. (2015), García-Fernández et al. (2015), Gašperin and Juričić (2011), and Schön et al. (2011) discuss a very similar approach to our GVI scheme in the context of nonlinear smoothers and filters; some of these works also carry out parameter estimation of the motion and observation models, which we also discuss as it fits neatly into the variational approach (Neal and Hinton 1998; Ghahramani and Roweis 1999). These works start from the same KL divergence, show how to exploit factorization of the joint likelihood, and discuss how to apply sigmapoints (Kokkala et al. 2014, 2016; Gašperin and Juričić 2011) or particles (Schön et al. 2011) to avoid the need to compute derivatives. García-Fernández et al. (2015) is a filtering paper that follows a similar philosophy to the current paper by statistically linearizing about an iteratively improved posterior. Our paper extends these works by (i) generalizing to any large-scale batch GVI problems where the likelihood can be factored (not restricted to smoothers with block-tridiagonal inverse covariance), (ii) devising a Newton-style iterative solver for both mean and inverse covariance, (iii) explicitly showing how to exploit problem-specific structure in the case of a factored likelihood to make the technique efficient, and (iv) demonstrating the approach on problems of interest in robotics.

There have been a few additional approaches to applying sampled-based techniques to batch estimation; however, they are quite different from ours. Park et al. (2009) and Roh et al. (2007) present a batch estimator that uses the sigmapoint Kalman filter framework as the optimization method. For each major iteration, they compute sigmapoints for the estimated mean and propagate them through the motion model over all time steps. Then, the measurements from all of these propagated sigmapoints are stacked in a large column vector and the standard

sigmapoint measurement update is applied. Although this method has been reported to work well (Park et al. 2009; Roh et al. 2007), it is expensive because it requires constructing the full covariance matrix to obtain the Kalman gain in the measurement update step. In this paper, we work with the inverse covariance matrix and show how to avoid ever constructing the full covariance matrix, which opens to the door to use on large-scale estimation problems.

3 Gaussian Variational Inference

This section poses the problem we are going to solve and proposes a general solution. Exploiting application-specific structure is discussed later, in Section 4. We first define the loss functional that we seek to minimize, then derive an optimization scheme in order to minimize it with respect to the parameters of a Gaussian. As an aside, we show that our optimization scheme is equivalent to so-called Natural Gradient Descent (NGD). Following this, we work our optimization scheme into a different form in preparation for exploiting application-specific structure and finally show that we can recover the classic RTS smoother in the linear case.

3.1 Loss Functional

As is common in variational inference (Bishop 2006), we seek to minimize the KL divergence (Kullback and Leibler 1951) between the true Bayesian posterior, $p(\mathbf{x}|\mathbf{z})$, and an approximation of the posterior, $q(\mathbf{x})$, which in our case will be a multivariate Gaussian PDF,

$$\begin{aligned} q(\mathbf{x}) &= \mathcal{N}(\boldsymbol{\mu}, \boldsymbol{\Sigma}) \\ &= \frac{1}{\sqrt{(2\pi)^N |\boldsymbol{\Sigma}|}} \exp \left(-\frac{1}{2} (\mathbf{x} - \boldsymbol{\mu})^T \boldsymbol{\Sigma}^{-1} (\mathbf{x} - \boldsymbol{\mu}) \right), \end{aligned} \quad (5)$$

where $|\cdot|$ is the determinant. For practical robotics and computer vision problems, the dimension of the state, N , can become very large and so the main point of our paper is to show how to carry out GVI in an efficient manner for large-scale problems*.

As KL divergence is not symmetrical, we have a choice of using $\text{KL}(p||q)$ or $\text{KL}(q||p)$. Bishop (2006, p. 467) provides a good discussion of the differences between these two functionals. The former expression is given by

$$\begin{aligned} \text{KL}(p||q) &= - \int_{-\infty}^{\infty} p(\mathbf{x}|\mathbf{z}) \ln \left(\frac{q(\mathbf{x})}{p(\mathbf{x}|\mathbf{z})} \right) d\mathbf{x} \\ &= \mathbb{E}_p [\ln p(\mathbf{x}|\mathbf{z}) - \ln q(\mathbf{x})], \end{aligned} \quad (6)$$

while the latter is

$$\begin{aligned} \text{KL}(q||p) &= - \int_{-\infty}^{\infty} q(\mathbf{x}) \ln \left(\frac{p(\mathbf{x}|\mathbf{z})}{q(\mathbf{x})} \right) d\mathbf{x} \\ &= \mathbb{E}_q [\ln q(\mathbf{x}) - \ln p(\mathbf{x}|\mathbf{z})], \end{aligned} \quad (7)$$

where $\mathbf{x} \in \mathbb{R}^N$ is the latent state that we seek to infer from data, $\mathbf{z} \in \mathbb{R}^D$, and $\mathbb{E}[\cdot]$ is the expectation operator. The key practical difference that leads us to choose $\text{KL}(q||p)$ is that the expectation is over our Gaussian estimate, $q(\mathbf{x})$, rather than the true posterior, $p(\mathbf{x}|\mathbf{z})$. We will show that we can use this fact to devise an efficient iterative scheme for $q(\mathbf{x})$ that best approximates the posterior. Moreover, our choice of $\text{KL}(q||p)$ leads naturally to also estimating parameters of the system (Neal and Hinton 1998), which we discuss in Section 5.2. Ranganathan et al. (2007) and Davison and Ortiz (2019) discuss approximate Gaussian inference for robotics problems using loopy belief propagation, which is based on $\text{KL}(p||q)$ (Bishop 2006, p. 505); their emphasis is on parallelizing the computations whereas we are focused on improving the estimate over MAP.

We observe that our chosen KL divergence can be written as

$$\begin{aligned} \text{KL}(q||p) &= \mathbb{E}_q [-\ln p(\mathbf{x}, \mathbf{z})] \\ &\quad - \underbrace{\frac{1}{2} \ln ((2\pi e)^N |\boldsymbol{\Sigma}|)}_{\text{entropy}} + \underbrace{\ln p(\mathbf{z})}_{\text{constant}}, \end{aligned} \quad (8)$$

where we have used the expression for the *entropy*, $-\int q(\mathbf{x}) \ln q(\mathbf{x}) d\mathbf{x}$, for a Gaussian. Noticing that the final term is a constant (i.e., it does not depend on $q(\mathbf{x})$) we define the following loss functional that we seek to minimize with respect to $q(\mathbf{x})$:

$$V(q) = \mathbb{E}_q [\phi(\mathbf{x})] + \frac{1}{2} \ln (|\boldsymbol{\Sigma}^{-1}|), \quad (9)$$

with $\phi(\mathbf{x}) = -\ln p(\mathbf{x}, \mathbf{z})$. We deliberately switch from $\boldsymbol{\Sigma}$ (covariance matrix) to $\boldsymbol{\Sigma}^{-1}$ (inverse covariance matrix also known as the *information matrix* or *precision matrix*) in (9) as the latter enjoys sparsity that the former does not; we will carry this forward and use $\boldsymbol{\mu}$ and $\boldsymbol{\Sigma}^{-1}$ as a complete description of $q(\mathbf{x})$. The first term in $V(q)$ encourages the solution to match the data while the second penalizes it for being too certain; although we did not experiment with this, a relative weighting (i.e., a metaparameter) between these two terms could be used to tune performance on other metrics of interest. It is also worth mentioning that $V(q)$ is the negative of the so-called Evidence Lower Bound (ELBO), which we will consequently minimize.

3.2 Optimization Scheme

Our next task is to define an optimization scheme to minimize the loss functional with respect to the mean, $\boldsymbol{\mu}$, and inverse covariance, $\boldsymbol{\Sigma}^{-1}$. Our approach will be similar to a Newton-style optimizer.

*Note, we choose not to make a mean-field approximation, instead allowing all variables to be correlated

After a bit of calculus, the derivatives of our loss functional, $V(q)$, with respect to our Gaussian parameters, $\boldsymbol{\mu}$ and $\boldsymbol{\Sigma}^{-1}$, are given by (Opper and Archambeau 2009)

$$\frac{\partial V(q)}{\partial \boldsymbol{\mu}^T} = \boldsymbol{\Sigma}^{-1} \mathbb{E}_q[(\mathbf{x} - \boldsymbol{\mu})\phi(\mathbf{x})], \quad (10a)$$

$$\begin{aligned} \frac{\partial^2 V(q)}{\partial \boldsymbol{\mu}^T \partial \boldsymbol{\mu}} &= \boldsymbol{\Sigma}^{-1} \mathbb{E}_q[(\mathbf{x} - \boldsymbol{\mu})(\mathbf{x} - \boldsymbol{\mu})^T \phi(\mathbf{x})] \boldsymbol{\Sigma}^{-1} \\ &\quad - \boldsymbol{\Sigma}^{-1} \mathbb{E}_q[\phi(\mathbf{x})], \end{aligned} \quad (10b)$$

$$\begin{aligned} \frac{\partial V(q)}{\partial \boldsymbol{\Sigma}^{-1}} &= -\frac{1}{2} \mathbb{E}_q[(\mathbf{x} - \boldsymbol{\mu})(\mathbf{x} - \boldsymbol{\mu})^T \phi(\mathbf{x})] \\ &\quad + \frac{1}{2} \boldsymbol{\Sigma} \mathbb{E}_q[\phi(\mathbf{x})] + \frac{1}{2} \boldsymbol{\Sigma}, \end{aligned} \quad (10c)$$

where, comparing (10b) and (10c), we notice that

$$\frac{\partial^2 V(q)}{\partial \boldsymbol{\mu}^T \partial \boldsymbol{\mu}} = \boldsymbol{\Sigma}^{-1} - 2\boldsymbol{\Sigma}^{-1} \frac{\partial V(q)}{\partial \boldsymbol{\Sigma}^{-1}} \boldsymbol{\Sigma}^{-1}. \quad (11)$$

This relationship is critical to defining our optimization scheme, which we do next.

To find extrema, we could attempt to set the first derivatives to zero, but it is not (in general) possible to isolate for $\boldsymbol{\mu}$ and $\boldsymbol{\Sigma}^{-1}$ in closed form. Hence, we will define an iterative update scheme. We begin by writing out a Taylor series expansion of $V(q)$ that is second order in $\delta\boldsymbol{\mu}$ but only first order in $\delta\boldsymbol{\Sigma}^{-1}$ (second order would be difficult to calculate and covariance quantities are already quadratic \mathbf{x}):

$$\begin{aligned} V(q^{(i+1)}) &\approx V(q^{(i)}) + \left(\frac{\partial V(q)}{\partial \boldsymbol{\mu}^T} \bigg|_{q^{(i)}} \right)^T \delta\boldsymbol{\mu} \\ &\quad + \frac{1}{2} \delta\boldsymbol{\mu}^T \left(\frac{\partial^2 V(q)}{\partial \boldsymbol{\mu}^T \partial \boldsymbol{\mu}} \bigg|_{q^{(i)}} \right) \delta\boldsymbol{\mu} \\ &\quad + \text{tr} \left(\frac{\partial V(q)}{\partial \boldsymbol{\Sigma}^{-1}} \bigg|_{q^{(i)}} \delta\boldsymbol{\Sigma}^{-1} \right), \end{aligned} \quad (12)$$

where $\delta\boldsymbol{\mu} = \boldsymbol{\mu}^{(i+1)} - \boldsymbol{\mu}^{(i)}$ and $\delta\boldsymbol{\Sigma}^{-1} = (\boldsymbol{\Sigma}^{-1})^{(i+1)} - (\boldsymbol{\Sigma}^{-1})^{(i)}$ with i the iteration index of our scheme. We now want to choose $\delta\boldsymbol{\mu}$ and $\delta\boldsymbol{\Sigma}^{-1}$ to force $V(q)$ to get smaller.

For the inverse covariance, $\boldsymbol{\Sigma}^{-1}$, if we set the derivative, $\frac{\partial V(q)}{\partial \boldsymbol{\Sigma}^{-1}}$, to zero (for an extremum) in (11) we immediately have

$$\boldsymbol{\Sigma}^{-1(i+1)} = \frac{\partial^2 V(q)}{\partial \boldsymbol{\mu}^T \partial \boldsymbol{\mu}} \bigg|_{q^{(i)}}, \quad (13)$$

where we place an index of $(i+1)$ on the left and (i) on the right in order to define an iterative update. Inserting (11) again on the right we see that the change to the inverse covariance by using this update can also be written as

$$\delta\boldsymbol{\Sigma}^{-1} = -2 (\boldsymbol{\Sigma}^{-1})^{(i)} \frac{\partial V(q)}{\partial \boldsymbol{\Sigma}^{-1}} \bigg|_{q^{(i)}} (\boldsymbol{\Sigma}^{-1})^{(i)}. \quad (14)$$

Convergence of this scheme will be discussed below[†].

For the mean, $\boldsymbol{\mu}$, we will take inspiration from the MAP approach to Gaussian nonlinear batch estimation and employ a Newton-style update (Nocedal and Wright 2006). Since our loss approximation (12) is locally quadratic in $\delta\boldsymbol{\mu}$, we take the derivative with respect to $\delta\boldsymbol{\mu}$ and set this to zero (to find the minimum). This results in a linear system of equations for $\delta\boldsymbol{\mu}$:

$$\underbrace{\left(\frac{\partial^2 V(q)}{\partial \boldsymbol{\mu}^T \partial \boldsymbol{\mu}} \bigg|_{q^{(i)}} \right)}_{(\boldsymbol{\Sigma}^{-1})^{(i+1)}} \delta\boldsymbol{\mu} = - \left(\frac{\partial V(q)}{\partial \boldsymbol{\mu}^T} \bigg|_{q^{(i)}} \right), \quad (15)$$

where we note the convenient reappearance of $\boldsymbol{\Sigma}^{-1}$ as the left-hand side.

Inserting our chosen scheme for $\delta\boldsymbol{\mu}$ and $\delta\boldsymbol{\Sigma}^{-1}$ into the loss approximation (12), we have

$$\begin{aligned} V(q^{(i+1)}) - V(q^{(i)}) &\approx -\frac{1}{2} \underbrace{\delta\boldsymbol{\mu}^T (\boldsymbol{\Sigma}^{-1})^{(i+1)} \delta\boldsymbol{\mu}}_{\geq 0} \\ &\quad \text{with equality iff } \delta\boldsymbol{\mu} = \mathbf{0} \\ &\quad - \frac{1}{2} \underbrace{\text{tr} \left((\boldsymbol{\Sigma}^{(i)} \delta\boldsymbol{\Sigma}^{-1} \boldsymbol{\Sigma}^{(i)} \delta\boldsymbol{\Sigma}^{-1}) \right)}_{\geq 0} \leq 0, \end{aligned} \quad (16)$$

with equality iff $\delta\boldsymbol{\Sigma}^{-1} = \mathbf{0}$
(see Appendix A)

which shows that we will reduce our loss, $V(q)$, so long as $\delta\boldsymbol{\mu}$ and $\delta\boldsymbol{\Sigma}^{-1}$ are not both zero; this is true when the derivatives with respect to $\boldsymbol{\mu}$ and $\boldsymbol{\Sigma}^{-1}$ are not both zero, which occurs only at a local minimum of $V(q)$. This is a local convergence guarantee only as the expression is based on our Taylor series expansion in (12).

3.3 Natural Gradient Descent Interpretation

As an aside, we can interpret our update for $\delta\boldsymbol{\mu}$ and $\delta\boldsymbol{\Sigma}^{-1}$ as carrying out so-called Natural Gradient Descent (NGD) (Amari 1998; Hoffman et al. 2013; Barfoot 2020), which

[†]It is worth mentioning that (10c) ignores the fact that $\boldsymbol{\Sigma}^{-1}$ is actually a symmetric matrix. Magnus and Neudecker (2019) discuss how to calculate the derivative of a function with respect to a matrix while accounting for its symmetry. They show that if \mathbf{A} is the derivative of a function (with respect to a symmetric matrix, \mathbf{B}) that ignores symmetry, then $\mathbf{A} + \mathbf{A}^T - \mathbf{A} \circ \mathbf{1}$ is the derivative accounting for the symmetry of \mathbf{B} , where \circ is the Hadamard (element-wise) product and $\mathbf{1}$ is the identity matrix. It is not too difficult to see that $\mathbf{A} = \mathbf{0}$ if and only if $\mathbf{A} + \mathbf{A}^T - \mathbf{A} \circ \mathbf{1} = \mathbf{0}$ in the case of a symmetric \mathbf{A} . Therefore, if we want to find an extremum by setting the derivative to zero, we can simply set $\mathbf{A} = \mathbf{0}$ as long as \mathbf{A} is symmetric and this will account for the symmetry of \mathbf{B} correctly. Barfoot (2020) investigates this issue more thoroughly.

exploits the information geometry to make the update more efficient than regular gradient descent. To see this, we stack our variational parameters into a single column, α , using the $\text{vec}(\cdot)$ operator, which converts a matrix to a vector by stacking its columns:

$$\alpha = \begin{bmatrix} \mu \\ \text{vec}(\Sigma^{-1}) \end{bmatrix}, \quad \delta\alpha = \begin{bmatrix} \delta\mu \\ \text{vec}(\delta\Sigma^{-1}) \end{bmatrix},$$

$$\frac{\partial V(q)}{\partial \alpha^T} = \begin{bmatrix} \frac{\partial V(q)}{\partial \mu^T} \\ \text{vec}\left(\frac{\partial V(q)}{\partial \Sigma^{-1}}\right) \end{bmatrix}. \quad (17)$$

The last expression is the gradient of the loss functional with respect to α .

The NGD update scheme can then be defined as

$$\delta\alpha = -\mathcal{I}_\alpha^{-1} \frac{\partial V(q)}{\partial \alpha^T}, \quad (18)$$

where \mathcal{I}_α is the Fisher Information Matrix (FIM) (Fisher 1922) for the variational parameter, α , and its calculation can be found in Appendix B. Inserting the details of the components of the above we have

$$\begin{bmatrix} \delta\mu \\ \text{vec}(\delta\Sigma^{-1}) \end{bmatrix} = - \begin{bmatrix} \Sigma^{-1} & \mathbf{0} \\ \mathbf{0} & \frac{1}{2}(\Sigma \otimes \Sigma) \end{bmatrix}^{-1} \begin{bmatrix} \frac{\partial V(q)}{\partial \mu^T} \\ \text{vec}\left(\frac{\partial V(q)}{\partial \Sigma^{-1}}\right) \end{bmatrix}, \quad (19)$$

where \otimes is the Kronecker product. Extracting the individual updates we see

$$\delta\mu = -\Sigma \frac{\partial V(q)}{\partial \mu^T}, \quad (20a)$$

$$\text{vec}(\delta\Sigma^{-1}) = -2(\Sigma^{-1} \otimes \Sigma^{-1}) \text{vec}\left(\frac{\partial V(q)}{\partial \Sigma^{-1}}\right). \quad (20b)$$

Finally, using that $\text{vec}(\mathbf{ABC}) \equiv (\mathbf{C}^T \otimes \mathbf{A}) \text{vec}(\mathbf{B})$, we have

$$\Sigma^{-1} \delta\mu = -\frac{\partial V(q)}{\partial \mu^T}, \quad (21a)$$

$$\delta\Sigma^{-1} = -2\Sigma^{-1} \frac{\partial V(q)}{\partial \Sigma^{-1}} \Sigma^{-1}, \quad (21b)$$

which is the same set of updates as in the previous subsection.

3.4 Stein's Lemma

While our iterative scheme could be implemented as is, it will be expensive (i.e., $O(N^3)$ per iteration) for large problems. The next section will show how to exploit sparsity to make the scheme efficient and, in preparation

for that, we will manipulate our update equations into a slightly different form using *Stein's lemma* (Stein 1981). In our notation, the lemma says

$$\mathbb{E}_q[(\mathbf{x} - \mu)f(\mathbf{x})] \equiv \Sigma \mathbb{E}_q \left[\frac{\partial f(\mathbf{x})}{\partial \mathbf{x}^T} \right], \quad (22)$$

where $q(\mathbf{x}) = \mathcal{N}(\mu, \Sigma)$ is a Gaussian random variable and $f(\cdot)$ is any nonlinear differentiable function. A double application of Stein's lemma also reveals

$$\begin{aligned} \mathbb{E}_q[(\mathbf{x} - \mu)(\mathbf{x} - \mu)^T f(\mathbf{x})] \\ \equiv \Sigma \mathbb{E}_q \left[\frac{\partial^2 f(\mathbf{x})}{\partial \mathbf{x}^T \partial \mathbf{x}} \right] \Sigma + \Sigma \mathbb{E}_q[f(\mathbf{x})], \end{aligned} \quad (23)$$

assuming $f(\cdot)$ is twice differentiable. Combining Stein's lemma with our loss derivatives in (10a), (10b), and (10c), we have the useful identities

$$\frac{\partial}{\partial \mu^T} \mathbb{E}_q[f(\mathbf{x})] \equiv \mathbb{E}_q \left[\frac{\partial f(\mathbf{x})}{\partial \mathbf{x}^T} \right], \quad (24a)$$

$$\begin{aligned} \frac{\partial^2}{\partial \mu^T \partial \mu} \mathbb{E}_q[f(\mathbf{x})] &\equiv \mathbb{E}_q \left[\frac{\partial^2 f(\mathbf{x})}{\partial \mathbf{x}^T \partial \mathbf{x}} \right] \\ &\equiv -2\Sigma^{-1} \left(\frac{\partial}{\partial \Sigma^{-1}} \mathbb{E}_q[f(\mathbf{x})] \right) \Sigma^{-1}, \end{aligned} \quad (24b)$$

which we will have occasion to use later on; Appendix D provides the derivations.

We can apply Stein's lemma from (22) and (23) to our optimization scheme in (13) and (15) to write the iterative updates compactly as

$$(\Sigma^{-1})^{(i+1)} = \mathbb{E}_{q^{(i)}} \left[\frac{\partial^2}{\partial \mathbf{x}^T \partial \mathbf{x}} \phi(\mathbf{x}) \right], \quad (25a)$$

$$(\Sigma^{-1})^{(i+1)} \delta\mu = -\mathbb{E}_{q^{(i)}} \left[\frac{\partial}{\partial \mathbf{x}^T} \phi(\mathbf{x}) \right], \quad (25b)$$

$$\mu^{(i+1)} = \mu^{(i)} + \delta\mu. \quad (25c)$$

Ala-Luhtala et al. (2015, App. C) also make use of Stein's lemma in this way in the context of Gaussian variational smoothers. In general, this iterative scheme will still be expensive for large problems and so we will look to exploit structure to make GVI more efficient. As only the first and second derivatives of $\phi(\mathbf{x})$ are required, we can drop any constant terms (i.e., the normalization constant of $p(\mathbf{x}, \mathbf{z})$).

Notably, our optimization scheme in (25) is identical to the MAP approach (with the Laplace covariance approximation) if we approximate the expectations using only the mean of $q(\mathbf{x})$. Thus, MAP with Laplace can be viewed as an approximation of the more general approach we discuss in this paper.

3.5 Recovery of the RTS Smoother

Before moving on, we briefly show that our GVI formulation produces the discrete-time RTS smoother result

in the linear case. As is shown by Barfoot (2017, §3, p. 44), the batch linear state estimation problem can be written in *lifted form* (i.e., at the trajectory level):

$$\mathbf{x} = \mathbf{A}(\mathbf{B}\mathbf{u} + \mathbf{w}), \quad (26a)$$

$$\mathbf{y} = \mathbf{C}\mathbf{x} + \mathbf{n}, \quad (26b)$$

where \mathbf{x} is the entire trajectory (states over time), \mathbf{u} are the control inputs, \mathbf{y} are the sensor outputs, $\mathbf{w} \sim \mathcal{N}(\mathbf{0}, \mathbf{Q})$ is process noise, $\mathbf{n} \sim \mathcal{N}(\mathbf{0}, \mathbf{R})$ is measurement noise, \mathbf{A} is the lifted transition matrix, \mathbf{B} is the lifted control matrix, and \mathbf{C} is the lifted observation matrix. We then have

$$\begin{aligned} \phi(\mathbf{x}) = & \frac{1}{2} (\mathbf{B}\mathbf{u} - \mathbf{A}^{-1}\mathbf{x})^T \mathbf{Q}^{-1} (\mathbf{B}\mathbf{u} - \mathbf{A}^{-1}\mathbf{x}) \\ & + \frac{1}{2} (\mathbf{y} - \mathbf{C}\mathbf{x})^T \mathbf{R}^{-1} (\mathbf{y} - \mathbf{C}\mathbf{x}). \end{aligned} \quad (27)$$

The expected derivatives can be calculated analytically for this linear problem:

$$\mathbb{E}_q \left[\frac{\partial^2}{\partial \mathbf{x}^T \partial \mathbf{x}} \phi(\mathbf{x}) \right] \quad (28a)$$

$$= \mathbf{A}^{-T} \mathbf{Q}^{-1} \mathbf{A}^{-1} + \mathbf{C}^T \mathbf{R}^{-1} \mathbf{C},$$

$$\mathbb{E}_q \left[\frac{\partial}{\partial \mathbf{x}^T} \phi(\mathbf{x}) \right] \quad (28b)$$

$$= -\mathbf{A}^{-T} \mathbf{Q}^{-1} (\mathbf{B}\mathbf{u} - \mathbf{A}^{-1}\boldsymbol{\mu}) - \mathbf{C}^T \mathbf{R}^{-1} (\mathbf{y} - \mathbf{C}\boldsymbol{\mu}).$$

At convergence, (28b) must be zero, so we have

$$\boldsymbol{\Sigma}^{-1} = \underbrace{\mathbf{A}^{-T} \mathbf{Q}^{-1} \mathbf{A}^{-1} + \mathbf{C}^T \mathbf{R}^{-1} \mathbf{C}}_{\text{block-tridiagonal}}, \quad (29a)$$

$$\boldsymbol{\Sigma}^{-1} \boldsymbol{\mu} = \mathbf{A}^{-T} \mathbf{Q}^{-1} \mathbf{B}\mathbf{u} + \mathbf{C}^T \mathbf{R}^{-1} \mathbf{y}, \quad (29b)$$

which can be solved efficiently for $\boldsymbol{\mu}$ due to the block-tridiagonal nature of $\boldsymbol{\Sigma}^{-1}$; from here, Barfoot (2017, §3, p.55) shows the algebraic equivalence of this form to the canonical RTS smoother. Thus, our GVI approach still reproduces the classic linear result. However, we can also now address nonlinear problems more completely than the MAP case.

4 Exact Sparsity

This section shows how to exploit application-specific structure to make the optimization scheme of the previous section efficient for large-scale problems. We first show that when the joint likelihood of the state and data can be factored, the calculation of the required expectations in our optimization scheme is exactly sparse, meaning we only need the marginals of the covariance associated with each factor. We then discuss how we can calculate these marginals efficiently from the inverse covariance, for any GVI problem. Finally, we show how to use sigmapoints drawn from these marginals to implement the full optimization scheme.

4.1 Factored Joint Likelihood

We have seen in the previous section that the iterative update scheme relies on calculating three expectations:

$$\underbrace{\mathbb{E}_q[\phi(\mathbf{x})]}_{\text{scalar}}, \quad \underbrace{\mathbb{E}_q \left[\frac{\partial}{\partial \mathbf{x}^T} \phi(\mathbf{x}) \right]}_{\text{column}}, \quad \underbrace{\mathbb{E}_q \left[\frac{\partial^2}{\partial \mathbf{x}^T \partial \mathbf{x}} \phi(\mathbf{x}) \right]}_{\text{matrix}}, \quad (30)$$

where we drop the iteration index for now. Let us now assume that the joint state/data likelihood can be factored such that we can write its negative log-likelihood as

$$\phi(\mathbf{x}) = \sum_{k=1}^K \phi_k(\mathbf{x}_k), \quad (31)$$

where $\phi_k(\mathbf{x}_k) = -\ln p(\mathbf{x}_k, \mathbf{z}_k)$ is the k th (negative log) factor expression, \mathbf{x}_k is a *subset* of variables in \mathbf{x} associated with the k th factor, and \mathbf{z}_k is a subset of the data in \mathbf{z} associated with the k th factor.

Let us consider the first (scalar) expectation in (30). We can insert the factored likelihood and see what happens:

$$\begin{aligned} \mathbb{E}_q[\phi(\mathbf{x})] &= \mathbb{E}_q \left[\sum_{k=1}^K \phi_k(\mathbf{x}_k) \right] \\ &= \sum_{k=1}^K \mathbb{E}_q[\phi_k(\mathbf{x}_k)] = \sum_{k=1}^K \mathbb{E}_{q_k}[\phi_k(\mathbf{x}_k)], \end{aligned} \quad (32)$$

where the last step is subtle but paramount: the expectation simplifies from being over $q = q(\mathbf{x})$, the full Gaussian estimate, to being over $q_k = q_k(\mathbf{x}_k)$, the *marginal* of the estimate for just the variables in each factor. This is not an approximation and the implications are many.

The other two expectations (column and matrix) in (30) enjoy similar simplifications and more, but require a bit more explanation. Let \mathbf{P}_k be a projection matrix such that it extracts \mathbf{x}_k from \mathbf{x} :

$$\mathbf{x}_k = \mathbf{P}_k \mathbf{x}. \quad (33)$$

Then inserting the factored expression into the second (column) expectation we have

$$\begin{aligned} \mathbb{E}_q \left[\frac{\partial}{\partial \mathbf{x}^T} \phi(\mathbf{x}) \right] &= \mathbb{E}_q \left[\frac{\partial}{\partial \mathbf{x}^T} \sum_{k=1}^K \phi_k(\mathbf{x}_k) \right] \\ &= \sum_{k=1}^K \mathbb{E}_q \left[\frac{\partial}{\partial \mathbf{x}^T} \phi_k(\mathbf{x}_k) \right] \\ &= \sum_{k=1}^K \mathbf{P}_k^T \mathbb{E}_q \left[\frac{\partial}{\partial \mathbf{x}_k^T} \phi_k(\mathbf{x}_k) \right] \\ &= \sum_{k=1}^K \mathbf{P}_k^T \mathbb{E}_{q_k} \left[\frac{\partial}{\partial \mathbf{x}_k^T} \phi_k(\mathbf{x}_k) \right]. \end{aligned} \quad (34)$$

For factor k , we are able to simplify the derivative from being with respect to \mathbf{x} , to being with respect to \mathbf{x}_k , since there is no dependence on the variables not in \mathbf{x}_k and hence the derivative with respect to those variables is zero; we use the projection matrix (as a dilation matrix) to map the derivative back into the appropriate rows of the overall result. After this, the expectation again simplifies to being with respect to $q_k = q_k(\mathbf{x}_k)$, the marginal of the estimate for just the variables in factor k . For the last (matrix) expectation we have a similar result:

$$\begin{aligned} \mathbb{E}_q \left[\frac{\partial^2}{\partial \mathbf{x}^T \partial \mathbf{x}} \phi(\mathbf{x}) \right] &= \mathbb{E}_q \left[\frac{\partial^2}{\partial \mathbf{x}^T \partial \mathbf{x}} \sum_{k=1}^K \phi_k(\mathbf{x}_k) \right] \\ &= \sum_{k=1}^K \mathbb{E}_q \left[\frac{\partial^2}{\partial \mathbf{x}^T \partial \mathbf{x}} \phi_k(\mathbf{x}_k) \right] \\ &= \sum_{k=1}^K \mathbf{P}_k^T \mathbb{E}_q \left[\frac{\partial^2}{\partial \mathbf{x}_k^T \partial \mathbf{x}_k} \phi_k(\mathbf{x}_k) \right] \mathbf{P}_k \\ &= \sum_{k=1}^K \mathbf{P}_k^T \mathbb{E}_{q_k} \left[\frac{\partial^2}{\partial \mathbf{x}_k^T \partial \mathbf{x}_k} \phi_k(\mathbf{x}_k) \right] \mathbf{P}_k. \end{aligned} \quad (35)$$

The simplified expectations in (32), (34), and (35) are the key tools that enable our ESGVI approach and we now make several remarks about them:

1. We do not require the full Gaussian estimate, $q(\mathbf{x})$, to evaluate the three expectations involved in our iterative scheme but rather we only require the marginals associated with each factor, $q_k(\mathbf{x}_k)$. This can represent a huge computational and storage savings in practical problems because it means that we never need to fully construct and store the (usually dense) covariance matrix, Σ . Schön et al. (2011); Gašperin and Juričić (2011); Kulkarni et al. (2016) also show how the required expectations are simplified to being over the marginals specifically for the smoother problem, but here we have generalized that result to any factorization of the joint likelihood.
2. Looking to the covariance update in (25a) and now the simplification in (35), we know that Σ^{-1} will be exactly sparse (with the pattern depending on the nature of the factors) and that *the sparsity pattern will remain constant as we iterate*. A fixed sparsity pattern ensures that we can build a custom sparse solver for the mean (25b) and use it safely at each iteration; for example, in the batch state estimation problem, Σ^{-1} is block-tridiagonal (under a chronological variable ordering).

3. As a reminder, marginalization of a Gaussian amounts to projection such that

$$q_k(\mathbf{x}_k) = \mathcal{N}(\boldsymbol{\mu}_k, \Sigma_{kk}) = \mathcal{N}(\mathbf{P}_k \boldsymbol{\mu}, \mathbf{P}_k \Sigma \mathbf{P}_k^T), \quad (36)$$

so that it is just specific sub-blocks of the full covariance matrix that are ever required.

4. The *only* sub-blocks of Σ that we require are precisely the ones corresponding to the non-zero sub-blocks of Σ^{-1} (which is typically highly sparse). We can see this more plainly by writing

$$\Sigma^{-1} = \sum_{k=1}^K \mathbf{P}_k^T \mathbb{E}_{q_k} \left[\frac{\partial^2}{\partial \mathbf{x}_k^T \partial \mathbf{x}_k} \phi_k(\mathbf{x}_k) \right] \mathbf{P}_k, \quad (37)$$

where we can see that each factor uses some sub-blocks, $\Sigma_{kk} = \mathbf{P}_k \Sigma \mathbf{P}_k^T$, to evaluate the expectation, and then the results are inserted back into the same elements of Σ^{-1} .

5. It turns out that we can extract the required sub-blocks of Σ very efficiently. For example, for batch state estimation, with a block-tridiagonal Σ^{-1} , we can piggyback the calculation of the required blocks (i.e., the three main block diagonals of Σ) onto the solution for the mean in (25b) (Meurant 1992; Barfoot 2017) while keeping the complexity of the solver the same. However, we can also compute the required blocks of Σ efficiently in the general case (Takahashi et al. 1973), and the next section is devoted to discussion of this topic.

Some of these remarks may seem familiar to those used to working with a MAP approach to batch state estimation (e.g., the sparsity pattern of Σ^{-1} exists and is constant across iterations). But now we are performing GVI that iterates over a full Gaussian PDF (i.e., mean and covariance) not just a point estimate (i.e., mean only).

At this point, the only approximation that we have made is that our estimate of the posterior is Gaussian. However, to implement the scheme in practice, we need to choose a method to actually compute the (marginal) expectations in (32), (34), and (35). There are many choices including linearization, Monte Carlo sampling, and also deterministic sampling. We will show how to use sampling methods in a later section.

4.2 Partial Computation of the Covariance

For completeness, we briefly summarize how it is possible to compute the blocks of Σ (typically dense) corresponding to the non-zero sub-blocks of Σ^{-1} (typically very sparse) in an efficient manner. This idea was first proposed by Takahashi et al. (1973) in the context of circuit theory and was later used by Broussolle (1978) in a state estimation context where the matrix of interest was a covariance matrix

$$\begin{aligned}
\begin{bmatrix} \ddots & & & \\ \dots & \Sigma_{K-2,K-2} & & \\ \dots & \Sigma_{K-1,K-2} & \Sigma_{K-1,K-1} & \\ \dots & \Sigma_{K,K-2} & \Sigma_{K,K-1} & \Sigma_{K,K} \end{bmatrix} &= \begin{bmatrix} \ddots & & & \\ \dots & \mathbf{D}_{K-2,K-2}^{-1} & & \\ \dots & \mathbf{0} & \mathbf{D}_{K-1,K-1}^{-1} & \\ \dots & \mathbf{0} & \mathbf{0} & \mathbf{D}_{K,K}^{-1} \end{bmatrix} \\
&- \begin{bmatrix} \ddots & \vdots & \vdots & \vdots \\ \dots & \Sigma_{K-2,K-2} & \Sigma_{K-2,K-1} & \Sigma_{K-2,K} \\ \dots & \Sigma_{K-1,K-2} & \Sigma_{K-1,K-1} & \Sigma_{K-1,K} \\ \dots & \Sigma_{K,K-2} & \Sigma_{K,K-1} & \Sigma_{K,K} \end{bmatrix} \begin{bmatrix} \ddots & & & \\ \dots & \mathbf{0} & & \\ \dots & \mathbf{L}_{K-1,K-2} & \mathbf{0} & \\ \dots & \mathbf{L}_{K,K-2} & \mathbf{L}_{K,K-1} & \mathbf{0} \end{bmatrix} \quad (45)
\end{aligned}$$

like ours. Erisman and Tinney (1975) provide a proof of the closure of the Takahashi et al. procedure and also discuss algorithmic complexity. More recently, Triggs et al. (2000, App. B.4) and Kaess and Dellaert (2009) discuss methods to calculate specific blocks of the covariance matrix efficiently from the inverse covariance for computer vision and robotics applications, but do not discuss doing so for the complete set of covariance blocks corresponding to the non-zero blocks of the inverse covariance matrix.

At each iteration of our GVI approach, we are required to solve a system of linear equations for the change in the mean:

$$\Sigma^{-1} \delta \mu = \mathbf{r}, \quad (38)$$

where \mathbf{r} is the right-hand side in (25b). We start by carrying out a sparse lower-diagonal-upper decomposition,

$$\Sigma^{-1} = \mathbf{L} \mathbf{D} \mathbf{L}^T, \quad (39)$$

where \mathbf{D} is diagonal and \mathbf{L} is lower-triangular with ones on the main diagonal (and sparse). The cost of this decomposition will depend on the nature of the prior and measurement factors. The key thing is that the sparsity pattern of \mathbf{L} is a direct function of the factors' variable dependencies and can be determined in advance; more on this below. We can then solve the following two systems of equations for the change in the mean:

$$(\mathbf{L} \mathbf{D}) \mathbf{v} = \mathbf{r}, \quad (\text{sparse forward substitution}) \quad (40)$$

$$\mathbf{L}^T \delta \mu = \mathbf{v}. \quad (\text{sparse backward substitution}) \quad (41)$$

To solve for the required blocks of Σ , we notice that

$$\mathbf{L} \mathbf{D} \mathbf{L}^T \Sigma = \mathbf{1}, \quad (42)$$

where $\mathbf{1}$ is the identity matrix. We can premultiply by the inverse of $\mathbf{L} \mathbf{D}$ to arrive at

$$\mathbf{L}^T \Sigma = \mathbf{D}^{-1} \mathbf{L}^{-1}, \quad (43)$$

where \mathbf{L}^{-1} will in general no longer be sparse. Taking the transpose and adding $\Sigma - \Sigma \mathbf{L}$ to both sides we have (Takahashi et al. 1973)

$$\Sigma = \mathbf{L}^{-T} \mathbf{D}^{-1} + \Sigma (\mathbf{1} - \mathbf{L}). \quad (44)$$

Since Σ is symmetric, we only require (at most) calculation of the main diagonal and the lower-half blocks and, as it turns out, this can also be done through a backward substitution pass. To see this we expand the lower-half blocks as in (45) at the top of the page, where we only show the blocks necessary for the calculation of the lower-half of Σ ; critically, \mathbf{L}^{-T} is unnecessary since it only affects the upper-half blocks of Σ and is therefore dropped. Temporarily ignoring the need to exploit sparsity, we see that we can calculate the lower-half blocks of Σ through backward substitution:

$$\Sigma_{K,K} = \mathbf{D}_{K,K}^{-1}, \quad (46a)$$

$$\Sigma_{K,K-1} = -\Sigma_{K,K} \mathbf{L}_{K,K-1}, \quad (46b)$$

$$\Sigma_{K-1,K-1} = \mathbf{D}_{K-1,K-1}^{-1} - \Sigma_{K-1,K} \mathbf{L}_{K,K-1}, \quad (46c)$$

$$\vdots$$

$$\Sigma_{j,k} = \delta(j,k) \mathbf{D}_{j,k}^{-1} - \sum_{\ell=k+1}^K \Sigma_{j,\ell} \mathbf{L}_{\ell,k}, \quad (j \geq k) \quad (46d)$$

where $\delta(\cdot, \cdot)$ is the Kronecker delta function.

In general, blocks that are zero in \mathbf{L} will also be zero in Σ^{-1} , but not the other way around. Therefore, it is sufficient (but not necessary) to calculate the blocks of Σ that are non-zero in \mathbf{L} and it turns out this can always be done. Table 1 shows some example sparsity patterns for Σ^{-1} and the corresponding sparsity pattern of \mathbf{L} . The sparsity of the lower-half of \mathbf{L} is the same as the sparsity of the lower-half of Σ^{-1} except that \mathbf{L} can have a few more non-zero entries to ensure that when multiplied together the sparsity of Σ^{-1} is produced. Specifically, if $\mathbf{L}_{k,i} \neq \mathbf{0}$ and $\mathbf{L}_{j,i} \neq \mathbf{0}$ then we must have $\mathbf{L}_{j,k} \neq \mathbf{0}$ (Erisman and Tinney 1975); this can be visualized as completing the ‘four corners of a box’, as shown in the example in the first column of Table 1.

Table 1 also shows some typical robotics examples. In batch trajectory estimation, Σ^{-1} is block-tridiagonal and in this case the \mathbf{L} matrix requires no extra non-zero entries. In SLAM, Σ^{-1} is an ‘arrowhead’ matrix with the upper-left partition (corresponding to the robot’s trajectory) as block-tridiagonal and the lower-right partition

Table 1. Example sparsity patterns of Σ^{-1} and the corresponding sparsity patterns of factor \mathbf{L} , where $*$ indicates non-zero. The set of zero entries of the lower-half of \mathbf{L} is a subset of the zero entries of the lower-half of Σ^{-1} . There are some extra non-zero entries of \mathbf{L} , shown as $+$, that arise from completing the ‘four corners of a box’. The box rule is shown in light grey for the leftmost example; the bottom-right corner of the box is zero in Σ^{-1} but non-zero in \mathbf{L} .

basic sparsity constraint (note fill in at (5, 3) in \mathbf{L})	trajectory example (6 robot poses)	SLAM example (3 poses, 3 landmarks)
$\Sigma^{-1} = \begin{bmatrix} * & & * & & * \\ & * & & & \\ * & & * & & \\ & & & * & \\ * & & & & * \end{bmatrix}$	$\Sigma^{-1} = \begin{bmatrix} * & * & & & & \\ * & * & * & & & \\ & * & * & * & & \\ & & * & * & * & \\ & & & * & * & * \\ & & & & * & * \end{bmatrix}$	$\Sigma^{-1} = \begin{bmatrix} * & * & & * & * & * \\ * & * & * & & * & * \\ * & * & * & & * & * \\ * & * & * & & * & * \\ * & * & * & & * & * \\ * & * & * & & * & * \end{bmatrix}$
$\mathbf{L} = \begin{bmatrix} * & & * & & \\ & * & & & \\ * & & * & & \\ & & & * & \\ * & & & & * \end{bmatrix}$	$\mathbf{L} = \begin{bmatrix} * & & & & & \\ * & * & & & & \\ & * & * & & & \\ & & * & * & & \\ & & & * & * & \\ & & & & * & * \end{bmatrix}$	$\mathbf{L} = \begin{bmatrix} * & & & & & \\ * & * & & & & \\ & * & * & & & \\ * & * & * & & * & \\ * & * & * & & + & * \\ * & * & * & & + & + \end{bmatrix}$

(corresponding to landmarks) as block-diagonal. Using an \mathbf{LDL}^T decomposition, we can exploit the sparsity of the upper-left partition, as shown in the example. If we wanted to exploit the sparsity of the lower-right, we could reverse the order of the variables or do a $\mathbf{L}^T \mathbf{DL}$ decomposition instead. In this SLAM example, each of the three landmarks is observed from each of the three poses so the upper-right and lower-left partitions are dense and this causes some extra entries of \mathbf{L} to be non-zero.

Finally, to understand why we do not need to calculate all of the blocks of Σ , we follow the explanation of Erisman and Tinney (1975). We aim to compute all the blocks of the lower-half of Σ corresponding to the non-zero blocks of \mathbf{L} . Looking to equation (46d), we see that if $\mathbf{L}_{p,k}$ is non-zero, then we require $\Sigma_{j,p}$ for the calculation of non-zero block $\Sigma_{j,k}$. But if $\Sigma_{j,k}$ is non-zero, so must be $\mathbf{L}_{j,k}$ and then using our ‘four corners of a box’ rule, this implies $\mathbf{L}_{j,p}$ must be non-zero and so we will have $\Sigma_{j,p}$ and $\Sigma_{p,j} = \Sigma_{j,p}^T$ on our list of blocks to compute already. This shows the calculation of the desired blocks is closed under the scheme defined by (46d), which in turn implies there will always exist an efficient algorithm to calculate the blocks of Σ corresponding to the non-zero blocks of Σ^{-1} , plus a few more according to the ‘four corners of a box’ rule.

It is worth noting that variable reordering and other schemes such as Givens rotations (Golub and Van Loan 1996) can be combined with the Takahashi et al. approach to maximize the benefit of sparsity in Σ^{-1} (Kaess et al. 2008). In this section, we have simply shown that in general, the calculation of the required blocks of Σ (corresponding to the non-zero block of Σ^{-1}) can be piggybacked efficiently onto the solution of (25b), with the details

depending on the specific problem. In fact, the bottleneck in terms of computational complexity is the original lower-diagonal-upper decomposition, which is typically required even for MAP approaches. We therefore claim that our ESGVI approach has the same order of computational cost (as a function of the state size, N) as MAP for a given problem, but will have a higher coefficient due to the extra burden of using the marginals to compute expectations.

4.3 Marginal Sampling

We have seen in the previous section that we actually only need to calculate the marginal expectations (for each factor),

$$\underbrace{\mathbb{E}_{q_k}[\phi_k(\mathbf{x}_k)]}_{\text{scalar}}, \quad \underbrace{\mathbb{E}_{q_k}\left[\frac{\partial}{\partial \mathbf{x}_k^T} \phi_k(\mathbf{x}_k)\right]}_{\text{column}}, \quad \underbrace{\mathbb{E}_{q_k}\left[\frac{\partial^2}{\partial \mathbf{x}_k^T \partial \mathbf{x}_k} \phi_k(\mathbf{x}_k)\right]}_{\text{matrix}}, \quad (47)$$

which can then be reassembled back into the larger expectations of (30).

As a quick aside, an additional use for the ‘scalar’ expression above is to evaluate the loss functional,

$$V(q) = \sum_{k=1}^K \underbrace{\mathbb{E}_{q_k}[\phi_k(\mathbf{x}_k)]}_{V_k(q_k)} + \underbrace{\frac{1}{2} \ln(|\Sigma^{-1}|)}_{V_0}, \quad (48)$$

which is used to test for convergence and to perform backtracking during optimization. The V_0 term can be

evaluated by noting that,

$$\ln(|\Sigma^{-1}|) = \ln(|\mathbf{LDL}^T|) = \ln(|\mathbf{D}|) = \sum_{i=1}^N \ln(d_{ii}), \quad (49)$$

where d_{ii} are the diagonal elements of \mathbf{D} ; this exploits the lower-diagonal-upper decomposition from (39) that we already compute during the optimization.

The computation of each expectation in (47) looks, on the surface, rather intimidating. The first and second derivatives suggests each factor must be twice differentiable, and somehow the expectation over $q_k(\mathbf{x}_k)$ must be computed. So far we have made no assumptions on the specific form of the factors ϕ_k , and we would like to keep it that way, avoiding the imposition of differentiability requirements. Additionally, recalling how sampling-based filters, such as the unscented Kalman filter (Julier and Uhlmann 1996), the cubature Kalman filter (Arasaratnam and Haykin 2009), and the Gauss-Hermite Kalman filter (Ito and Xiong 2000)(Wu et al. 2006), approximate terms involving expectations, a cubature approximation of the associated expectations in (47) appears appropriate. This section considers the use of Stein's lemma and cubature methods to derive an alternative means to compute the terms in (47) that is derivative-free.

To avoid the need to compute derivatives of ϕ_k , we can once again apply Stein's lemma, but in the opposite direction from our previous use. Using (22) we have

$$\mathbb{E}_{q_k} \left[\frac{\partial}{\partial \mathbf{x}_k^T} \phi_k(\mathbf{x}_k) \right] = \Sigma_{kk}^{-1} \mathbb{E}_{q_k} [(\mathbf{x}_k - \boldsymbol{\mu}_k) \phi_k(\mathbf{x}_k)], \quad (50)$$

and using (23) we have

$$\begin{aligned} \mathbb{E}_{q_k} \left[\frac{\partial^2}{\partial \mathbf{x}_k^T \partial \mathbf{x}_k} \phi_k(\mathbf{x}_k) \right] \\ = \Sigma_{kk}^{-1} \mathbb{E}_{q_k} [(\mathbf{x}_k - \boldsymbol{\mu}_k)(\mathbf{x}_k - \boldsymbol{\mu}_k)^T \phi_k(\mathbf{x}_k)] \Sigma_{kk}^{-1} \\ - \Sigma_{kk}^{-1} \mathbb{E}_{q_k} [\phi_k(\mathbf{x}_k)]. \end{aligned} \quad (51)$$

Thus, an alternative means to computing the three expectations in (47), without explicit computation of derivatives, involves first computing

$$\underbrace{\mathbb{E}_{q_k} [\phi_k(\mathbf{x}_k)]}_{\text{scalar}}, \quad \underbrace{\mathbb{E}_{q_k} [(\mathbf{x}_k - \boldsymbol{\mu}_k) \phi_k(\mathbf{x}_k)]}_{\text{column}}, \quad \underbrace{\mathbb{E}_{q_k} [(\mathbf{x}_k - \boldsymbol{\mu}_k)(\mathbf{x}_k - \boldsymbol{\mu}_k)^T \phi_k(\mathbf{x}_k)]}_{\text{matrix}}, \quad (52)$$

then computing (50) and (51) using the results of (52). The reverse application of Stein's lemma has not destroyed the sparsity that we unveiled earlier because we have now applied it at the marginal level, not the global level.

Of interest next is how to actually compute the three expectations given in (52) in an efficient yet accurate way. As integrals, the expectations in (52) are

$$\mathbb{E}_{q_k} [\phi_k(\mathbf{x}_k)] \quad (53a)$$

$$= \int_{-\infty}^{\infty} \phi_k(\mathbf{x}_k) q_k(\mathbf{x}_k) d\mathbf{x}_k,$$

$$\mathbb{E}_{q_k} [(\mathbf{x}_k - \boldsymbol{\mu}_k) \phi_k(\mathbf{x}_k)] \quad (53b)$$

$$= \int_{-\infty}^{\infty} (\mathbf{x}_k - \boldsymbol{\mu}_k) \phi_k(\mathbf{x}_k) q_k(\mathbf{x}_k) d\mathbf{x}_k,$$

$$\mathbb{E}_{q_k} [(\mathbf{x}_k - \boldsymbol{\mu}_k)(\mathbf{x}_k - \boldsymbol{\mu}_k)^T \phi_k(\mathbf{x}_k)] \quad (53c)$$

$$= \int_{-\infty}^{\infty} (\mathbf{x}_k - \boldsymbol{\mu}_k)(\mathbf{x}_k - \boldsymbol{\mu}_k)^T \phi_k(\mathbf{x}_k) q_k(\mathbf{x}_k) d\mathbf{x}_k,$$

where $q_k(\mathbf{x}_k) = \mathcal{N}(\boldsymbol{\mu}_k, \Sigma_{kk})$. Computing these integrals analytically is generally not possible, and as such, a numerical approximation is sought. There are many ways of approximating the integrals in (53), the most popular type being multi-dimensional *Gaussian quadrature*, commonly referred to as Gaussian cubature or simply *cubature* (Cools 1997)(Sarmavuori and Särkkä 2012)(Kokkala et al. 2016)(Särkkä et al. 2016)(Särkkä 2013, §6, p. 100). Using cubature, each of the integrals in (53) is approximated as (Kokkala et al. 2016)(Särkkä et al. 2016)(Särkkä 2013, §6, p. 99-106)

$$\mathbb{E}_{q_k} [\phi_k(\mathbf{x}_k)] \quad (54a)$$

$$\approx \sum_{\ell=1}^L w_{k,\ell} \phi_k(\mathbf{x}_{k,\ell}),$$

$$\mathbb{E}_{q_k} [(\mathbf{x}_k - \boldsymbol{\mu}_k) \phi_k(\mathbf{x}_k)] \quad (54b)$$

$$\approx \sum_{\ell=1}^L w_{k,\ell} (\mathbf{x}_{k,\ell} - \boldsymbol{\mu}_k) \phi_k(\mathbf{x}_{k,\ell}),$$

$$\mathbb{E}_{q_k} [(\mathbf{x}_k - \boldsymbol{\mu}_k)(\mathbf{x}_k - \boldsymbol{\mu}_k)^T \phi_k(\mathbf{x}_k)] \quad (54c)$$

$$\approx \sum_{\ell=1}^L w_{k,\ell} (\mathbf{x}_{k,\ell} - \boldsymbol{\mu}_k)(\mathbf{x}_{k,\ell} - \boldsymbol{\mu}_k)^T \phi_k(\mathbf{x}_{k,\ell}),$$

where $w_{k,\ell}$ are weights, $\mathbf{x}_{k,\ell} = \boldsymbol{\mu}_k + \sqrt{\Sigma_{kk}} \boldsymbol{\xi}_{k,\ell}$ are sigmapoints, and $\boldsymbol{\xi}_{k,\ell}$ are unit sigmapoints. Both the weights and unit sigmapoints are specific to the cubature method. For example, the popular unscented transformation (Julier and Uhlmann 1996)(Särkkä et al. 2016)(Särkkä 2013, §6, p. 109-110) uses weights

$$w_{k,0} = \frac{\kappa}{N_k + \kappa}, \quad w_{k,\ell} = \frac{1}{2(N_k + \kappa)}, \quad \ell = 1, \dots, 2N_k \quad (55)$$

and sigmapoints

$$\boldsymbol{\xi}_{k,\ell} = \begin{cases} \mathbf{0} & \ell = 0 \\ \sqrt{N_k + \kappa} \mathbf{1}_\ell & \ell = 1, \dots, N_k \\ -\sqrt{N_k + \kappa} \mathbf{1}_{\ell - N_k} & \ell = N_k + 1, \dots, 2N_k \end{cases}, \quad (56)$$

where N_k is the dimension of \mathbf{x}_k . On the other hand, the spherical-cubature rule (Arasaratnam and Haykin 2009)(Kokkala et al. 2016)(Särkkä 2013, §6, p. 106-109) uses weights

$$w_{k,\ell} = \frac{1}{2N_k}, \quad \ell = 1, \dots, 2N_k, \quad (57)$$

and sigmapoints

$$\boldsymbol{\xi}_{k,\ell} = \begin{cases} \sqrt{N_k} \mathbf{1}_\ell & \ell = 1, \dots, N_k \\ -\sqrt{N_k} \mathbf{1}_{\ell-N_k} & \ell = N_k + 1, \dots, 2N_k \end{cases}, \quad (58)$$

where $\mathbf{1}_i$ is a $N_k \times 1$ column matrix with 1 at row i and zeros everywhere else. Gauss-Hermite cubature is yet another method that can be used to compute the approximations in (54) (Ito and Xiong 2000)(Wu et al. 2006)(Särkkä 2013, §6 p. 99-106). As discussed in Särkkä (2013, §6 p. 103), given an integrand composed of a linear combination of monomials of the form $x_1^{d_1}, x_2^{d_2}, \dots, x_{N_k}^{d_{N_k}}$, the M th order Gauss-Hermite cubature rule is exact when $d_i \leq 2M - 1$. However, for an M th-order Gauss-Hermite cubature approximation, M^{N_k} sigmapoints are needed, which could be infeasible in practise when N_k is large (Särkkä 2013, §6 p. 103). Fortunately, the approximations of (53) given in (54) are at the factor level (i.e., at the level of \mathbf{x}_k , not \mathbf{x}), and at the factor level N_k is often a manageable size in most robotics problems. For this reason, Gauss-Hermite cubature is used in our numerical work presented in Sections 6.1, 6.2, and 6.3, yielding accurate yet reasonably efficient approximations of (53).

Some additional remarks are as follows:

1. The accuracy of the cubature approximations in (54) will depend on the specific method and the severity of the nonlinearity in ϕ_k . Alternative means to approximate (54), such as cubature methods that are exact for specific algebraic and trigonometric polynomials (Cools 1997)(Kokkala et al. 2016), Gaussian-process cubature (O’Hagan 1991)(Särkkä et al. 2016), or even adaptive cubature methods (Press et al. 2007, §4, p. 194), can be employed. In the case where computational complexity is of concern, a high-degree cubature rule that is an efficient alternative to Gauss-Hermite cubature is presented in Jia et al. (2013).
2. We are proposing quite a different way of using a cubature method (or any sampling method) than is typical in the state estimation literature; we consider the entire factor expression, ϕ_k , to be the nonlinearity, not just the observation or motion models, as is common. This means, for example, that if there is a robust cost function incorporated in our factor expression (Barfoot 2017, §5, p. 163)(MacTavish and Barfoot 2015), it is handled automatically and does

not need to be implemented as iteratively reweighted least squares (Holland and Welsch 1977).

3. Because we have ‘undone’ Stein’s lemma at this point (it was a temporary step to exploit the sparsity only), it may not even be necessary to have ϕ_k differentiable anymore. Appendix C shows how to get to the derivative-free version of ESGVI directly without the double application of Stein’s lemma. This opens the door to some interesting possibilities including the use of the H_∞ (worst case) norm, hard constraints on some or all of the states, or the aforementioned use of a robust cost function, within the factor ϕ_k . An appropriate sampling method would be required.
4. We see in (54) that the scalars, ϕ_k , serve to reweight each sample, but that otherwise the expressions are simply those for the first three moments of a distribution.
5. We also use cubature to evaluate $V(q)$ according to (48). This is required to test for convergence of the optimization scheme.

The approach that we have presented up to this point is extremely general and can benefit any GVI problem where $p(\mathbf{x}, \mathbf{z})$ can be factored. In computer vision and robotics, some examples include BA (Brown 1958) and SLAM (Durrant-Whyte and Bailey 2006). In Section 6, we will demonstrate the technique first on controlled toy problems, then on a batch SLAM problem.

5 Extensions

Before moving on to our experiments, we pause to elaborate two extensions of the main paper. First, we discuss an alternate loss functional that leads to a modified optimization scheme similar to a Gauss-Newton solver and offers some computational savings. Second, we discuss how to extend our approach beyond estimation of the latent state to include estimation of unknown parameters in our models.

5.1 Alternate Loss Functional

We can consider an alternate variational problem that may offer computational advantages over the main ESGVI approach of this paper. We consider the special case where the negative-log-likelihood takes the form

$$\phi(\mathbf{x}) = \frac{1}{2} \mathbf{e}(\mathbf{x})^T \mathbf{W}^{-1} \mathbf{e}(\mathbf{x}). \quad (59)$$

Substituting this into the loss functional, we have

$$V(q) = \frac{1}{2} \mathbb{E}_q [\mathbf{e}(\mathbf{x})^T \mathbf{W}^{-1} \mathbf{e}(\mathbf{x})] + \frac{1}{2} \ln(|\boldsymbol{\Sigma}^{-1}|). \quad (60)$$

Owing to the convexity of the quadratic expression, $\mathbf{e}^T \mathbf{W}^{-1} \mathbf{e}$, we can apply *Jensen’s inequality* (Jensen 1906)

directly to write

$$\mathbb{E}_q[\mathbf{e}(\mathbf{x})]^T \mathbf{W}^{-1} \mathbb{E}_q[\mathbf{e}(\mathbf{x})] \leq \mathbb{E}_q[\mathbf{e}(\mathbf{x})^T \mathbf{W}^{-1} \mathbf{e}(\mathbf{x})]. \quad (61)$$

The *Jensen gap* is the (positive) difference between the right and left sides of this inequality and will generally tend to be larger the more nonlinear is $\mathbf{e}(\mathbf{x})$ and less concentrated is $q(\mathbf{x})$. Motivated by this relationship, we can define a new loss functional as

$$V'(q) = \frac{1}{2} \mathbb{E}_q[\mathbf{e}(\mathbf{x})]^T \mathbf{W}^{-1} \mathbb{E}_q[\mathbf{e}(\mathbf{x})] + \frac{1}{2} \ln(|\Sigma^{-1}|), \quad (62)$$

which may be thought of as a (conservative) approximation of $V(q)$ that is appropriate for mild nonlinearities and/or concentrated posteriors; the conservative aspect will be discussed a bit later on. We will now show that we can minimize $V'(q)$ by iteratively updating $q(\mathbf{x})$ and continue to exploit problem sparsity arising from a factored likelihood.

We begin by noting that we can directly approximate the expected error as

$$\begin{aligned} \mathbb{E}_{q^{(i+1)}}[\mathbf{e}(\mathbf{x})] &\approx \mathbb{E}_{q^{(i)}}[\mathbf{e}(\mathbf{x})] + \frac{\partial}{\partial \boldsymbol{\mu}} \mathbb{E}_{q^{(i)}}[\mathbf{e}(\mathbf{x})] \underbrace{(\boldsymbol{\mu}^{(i+1)} - \boldsymbol{\mu}^{(i)})}_{\delta \boldsymbol{\mu}} \\ &= \underbrace{\mathbb{E}_{q^{(i)}}[\mathbf{e}(\mathbf{x})]}_{\bar{\mathbf{e}}^{(i)}} + \underbrace{\mathbb{E}_{q^{(i)}} \left[\frac{\partial}{\partial \mathbf{x}} \mathbf{e}(\mathbf{x}) \right]}_{\bar{\mathbf{E}}^{(i)}} \delta \boldsymbol{\mu} \\ &= \bar{\mathbf{e}}^{(i)} + \bar{\mathbf{E}}^{(i)} \delta \boldsymbol{\mu}, \end{aligned} \quad (63)$$

where we have employed the derivative identity in (24a).

We can then approximate the loss functional as

$$V'(q) \approx \frac{1}{2} \left(\bar{\mathbf{e}}^{(i)} + \bar{\mathbf{E}}^{(i)} \delta \boldsymbol{\mu} \right)^T \mathbf{W}^{-1} \left(\bar{\mathbf{e}}^{(i)} + \bar{\mathbf{E}}^{(i)} \delta \boldsymbol{\mu} \right) + \frac{1}{2} \ln(|\Sigma^{-1}|), \quad (64)$$

which is now exactly quadratic in $\delta \boldsymbol{\mu}$. This specific approximation leads directly to a Gauss-Newton estimator, bypassing Newton's method, as we have implicitly approximated the Hessian (Barfoot 2017, p.131). Taking the first and second derivatives with respect to $\delta \boldsymbol{\mu}$, we have

$$\frac{\partial V'(q)}{\partial \delta \boldsymbol{\mu}^T} = \bar{\mathbf{E}}^{(i)T} \mathbf{W}^{-1} \left(\bar{\mathbf{e}}^{(i)} + \bar{\mathbf{E}}^{(i)} \delta \boldsymbol{\mu} \right), \quad (65a)$$

$$\frac{\partial^2 V'(q)}{\partial \delta \boldsymbol{\mu}^T \partial \delta \boldsymbol{\mu}} = \bar{\mathbf{E}}^{(i)T} \mathbf{W}^{-1} \bar{\mathbf{E}}^{(i)}. \quad (65b)$$

For the derivative with respect to Σ^{-1} , we have

$$\frac{\partial V'(q)}{\partial \Sigma^{-1}} \approx -\frac{1}{2} \Sigma \bar{\mathbf{E}}^{(i)T} \mathbf{W}^{-1} \bar{\mathbf{E}}^{(i)} \Sigma + \frac{1}{2} \Sigma, \quad (66)$$

where the approximation enforces the relationship in (24b), which does not hold exactly anymore due to the altered nature of $V'(q)$. Setting this to zero for a critical point we have

$$(\Sigma^{-1})^{(i+1)} = \bar{\mathbf{E}}^{(i)T} \mathbf{W}^{-1} \bar{\mathbf{E}}^{(i)}, \quad (67)$$

where we have created an iterative update analogous to that in the main ESGVI approach.

For the mean, we set (65a) to zero and then for the optimal update we have

$$\underbrace{\bar{\mathbf{E}}^{(i)T} \mathbf{W}^{-1} \bar{\mathbf{E}}^{(i)}}_{(\Sigma^{-1})^{(i+1)}} \delta \boldsymbol{\mu} = -\bar{\mathbf{E}}^{(i)T} \mathbf{W}^{-1} \bar{\mathbf{e}}^{(i)}. \quad (68)$$

Solving for $\delta \boldsymbol{\mu}$ provides a Gauss-Newton update, which we will refer to as ESGVI Gauss-Newton (ESGVI-GN). This is identical to how Gauss-Newton is normally carried out, but now we calculate $\bar{\mathbf{e}}$ and $\bar{\mathbf{E}}$ not just at a single point but rather as an expectation over our Gaussian posterior estimate. We again make a number of remarks about the approach:

1. The sparsity of the inverse covariance matrix, Σ^{-1} , will be identical to the full ESGVI approach. This can be seen by noting that

$$\begin{aligned} \phi(\mathbf{x}) &= \sum_{k=1}^K \phi_k(\mathbf{x}_k) = \frac{1}{2} \sum_{k=1}^K \mathbf{e}_k(\mathbf{x}_k)^T \mathbf{W}_k^{-1} \mathbf{e}_k(\mathbf{x}_k) \\ &= \frac{1}{2} \mathbf{e}(\mathbf{x})^T \mathbf{W}^{-1} \mathbf{e}(\mathbf{x}), \end{aligned} \quad (69)$$

where

$$\mathbf{e}(\mathbf{x}) = \begin{bmatrix} \mathbf{e}_1(\mathbf{x}_1) \\ \vdots \\ \mathbf{e}_K(\mathbf{x}_K) \end{bmatrix}, \quad \mathbf{W} = \text{diag}(\mathbf{W}_1, \dots, \mathbf{W}_K). \quad (70)$$

Then we have

$$\begin{aligned} \Sigma^{-1} &= \mathbb{E}_q \left[\frac{\partial}{\partial \mathbf{x}} \mathbf{e}(\mathbf{x}) \right]^T \mathbf{W}^{-1} \mathbb{E}_q \left[\frac{\partial}{\partial \mathbf{x}} \mathbf{e}(\mathbf{x}) \right] \\ &= \sum_{k=1}^K \mathbf{P}_k^T \mathbb{E}_{q_k} \left[\frac{\partial}{\partial \mathbf{x}_k} \mathbf{e}_k(\mathbf{x}_k) \right]^T \mathbf{W}_k^{-1} \\ &\quad \times \mathbb{E}_{q_k} \left[\frac{\partial}{\partial \mathbf{x}_k} \mathbf{e}_k(\mathbf{x}_k) \right] \mathbf{P}_k, \end{aligned} \quad (71)$$

which will have zeros wherever an error term does not depend on the variables. We also see, just as before, that the expectations can be reduced to being over the marginal, $q_k(\mathbf{x}_k)$, meaning we still only require the blocks of Σ corresponding to the non-zero blocks of Σ^{-1} .

2. We can still use Stein's lemma to avoid the need to compute any derivatives:

$$\begin{aligned} \mathbb{E}_{q_k} \left[\frac{\partial}{\partial \mathbf{x}_k} \mathbf{e}_k(\mathbf{x}_k) \right] \\ = \mathbb{E}_{q_k} [\mathbf{e}_k(\mathbf{x}_k)(\mathbf{x}_k - \boldsymbol{\mu}_k)^T] \boldsymbol{\Sigma}_{kk}^{-1}. \end{aligned} \quad (72)$$

This is sometimes referred to as a statistical Jacobian and this usage is very similar to the filtering and smoothing approaches described by Särkkä (2013), amongst others, as cubature can be applied at the measurement model level rather than the factor level. Because we are iteratively recomputing the statistical Jacobian about our posterior estimate, this is most similar to Sibley et al. (2006) and García-Fernández et al. (2015), although some details are different as well as the fact that we started from our loss functional, $V'(q)$.

3. The number of cubature points required to calculate $\mathbb{E}_{q_k} [\mathbf{e}_k(\mathbf{x}_k)(\mathbf{x}_k - \boldsymbol{\mu}_k)^T]$ will be lower than our full ESGVI approach described earlier as the order of the expression in the integrand is half that of $\mathbb{E}_{q_k} [(\mathbf{x}_k - \boldsymbol{\mu}_k)(\mathbf{x}_k - \boldsymbol{\mu}_k)^T \phi_k(\mathbf{x}_k)]$. Since the number of cubature points goes up as M^{N_k} , cutting M in half is significant and could be the difference between tractable and not for some problems. This was the main motivation for exploring this alternate approach.
4. It is known that minimizing $\text{KL}(q||p)$, which our $V(q)$ is effectively doing, can result in a Gaussian that is too confident (i.e., inverse covariance is too large) (Bishop 2006; Ala-Luhtala et al. 2015). A side benefit of switching from $V(q)$ to $V'(q)$ is that the resulting inverse covariance will be more conservative. This follows from Jensen's inequality once again. For an arbitrary non-zero vector, \mathbf{a} , we have

$$\begin{aligned} 0 &< \mathbf{a}^T \underbrace{\mathbb{E}_q \left[\frac{\partial \mathbf{e}(\mathbf{x})}{\partial \mathbf{x}} \right]^T \mathbf{W}^{-1} \mathbb{E}_q \left[\frac{\partial \mathbf{e}(\mathbf{x})}{\partial \mathbf{x}} \right]}_{\boldsymbol{\Sigma}^{-1} \text{ from } V'(q)} \mathbf{a} \\ &\stackrel{\text{Jensen}}{\leq} \mathbf{a}^T \mathbb{E}_q \left[\frac{\partial \mathbf{e}(\mathbf{x})}{\partial \mathbf{x}}^T \mathbf{W}^{-1} \frac{\partial \mathbf{e}(\mathbf{x})}{\partial \mathbf{x}} \right] \mathbf{a} \\ &\stackrel{\text{Gauss-Newton}}{\approx} \mathbf{a}^T \underbrace{\mathbb{E}_q \left[\frac{\partial^2 \phi(\mathbf{x})}{\partial \mathbf{x}^T \partial \mathbf{x}} \right]}_{\boldsymbol{\Sigma}^{-1} \text{ from } V(q)} \mathbf{a}, \end{aligned} \quad (73)$$

which ensures that not only do we have a positive definite inverse covariance but that it is conservative compared to the full ESGVI approach.

Due to the extra approximations made in ESGVI-GN compared to ESGVI, it remains to be seen whether it

offers an improvement over MAP approaches. However, as ESGVI-GN provides a batch option that does not require any derivatives, it can be used as a less expensive preprocessor for the derivative-free version of full ESGVI.

5.2 Parameter Estimation

Although it is not the main focus of our paper, we use this section to provide a sketch of how parameters may also be estimated using our ESGVI framework. We introduce some unknown parameters, $\boldsymbol{\theta}$, to our loss functional,

$$V(q|\boldsymbol{\theta}) = \mathbb{E}_q[\phi(\mathbf{x}|\boldsymbol{\theta})] + \frac{1}{2} \ln(|\boldsymbol{\Sigma}^{-1}|), \quad (74)$$

and recall that $V(q|\boldsymbol{\theta})$ is the negative of the so-called Evidence Lower Bound (ELBO), which can be used in an Expectation Maximization (EM) framework to estimate parameters when there is a latent state (Neal and Hinton 1998; Ghahramani and Roweis 1999). The expectation, or E-step, is already accomplished by ESGVI; we simply hold $\boldsymbol{\theta}$ fixed and run the inference to convergence to solve for $q(\mathbf{x})$, our Gaussian approximation to the posterior. In the M-step, which is actually a minimization in our case, we hold $q(\mathbf{x})$ fixed and find the value of $\boldsymbol{\theta}$ that minimizes the loss functional. By alternating between the E- and M-steps, we can solve for the best value of the parameters to minimize $-\ln p(\mathbf{z}|\boldsymbol{\theta})$, the negative log-likelihood of the measurements given the parameters.

As we have done in the main part of the paper, we assume the joint likelihood of the state and measurements (given the parameters) factors so that

$$\phi(\mathbf{x}|\boldsymbol{\theta}) = \sum_{k=1}^K \phi_k(\mathbf{x}_k|\boldsymbol{\theta}), \quad (75)$$

where for generality we have each factor being affected by the entire parameter set, $\boldsymbol{\theta}$, but in practice it could be a subset. Taking the derivative of the loss functional with respect to $\boldsymbol{\theta}$, we have

$$\begin{aligned} \frac{\partial V(q|\boldsymbol{\theta})}{\partial \boldsymbol{\theta}} &= \frac{\partial}{\partial \boldsymbol{\theta}} \mathbb{E}_q[\phi(\mathbf{x}|\boldsymbol{\theta})] \\ &= \frac{\partial}{\partial \boldsymbol{\theta}} \mathbb{E}_q \left[\sum_{k=1}^K \phi_k(\mathbf{x}_k|\boldsymbol{\theta}) \right] \\ &= \sum_{k=1}^K \mathbb{E}_{q_k} \left[\frac{\partial}{\partial \boldsymbol{\theta}} \phi_k(\mathbf{x}_k|\boldsymbol{\theta}) \right], \end{aligned} \quad (76)$$

where in the last expression the expectation simplifies to being over the marginal, $q_k(\mathbf{x}_k)$, rather than the full Gaussian, $q(\mathbf{x})$. As with the main ESGVI approach, this means that we only need the blocks of the covariance, $\boldsymbol{\Sigma}$, corresponding to the non-zero blocks of $\boldsymbol{\Sigma}^{-1}$, which we are already calculating as part of the E-step. Furthermore,

Table 2. Descriptions of variants of our ESGVI algorithm tested in our experiments. The first two algorithms in the table are MAP comparisons, which can be recovered in our framework by evaluating all the expectations using a single quadrature point at the mean of the current estimate. The only extra feature added to the all the methods beyond the ‘plain vanilla’ implementation described in the theory section is that all algorithms are allowed to backtrack when updating the mean and inverse covariance in order to ensure that the loss functional actually decreases at each iteration.

algorithm label	method to evaluate expectations in (47)	M , number of quadrature points (per dimension)
MAP Newton	analytical Jacobian and Hessian	1
MAP GN	analytical Jacobian and approximate Hessian	1
ESGVI deriv $M=2$	analytical Jacobian and Hessian + quadrature	2
ESGVI deriv $M=3$	analytical Jacobian and Hessian + quadrature	3
ESGVI deriv-free $M=3$	Stein’s lemma + quadrature	3
ESGVI-GN deriv-free $M=3$	Stein’s lemma + quadrature	3
ESGVI deriv-free $M=4$	Stein’s lemma + quadrature	4
ESGVI deriv-free $M=10$	Stein’s lemma + quadrature	10

we can easily evaluate the marginal expectations using cubature.

To make this more tangible, consider the example of

$$\phi(\mathbf{x}|\mathbf{W}) = \frac{1}{2} \sum_{k=1}^K (\mathbf{e}_k(\mathbf{x}_k)^T \mathbf{W}^{-1} \mathbf{e}_k(\mathbf{x}_k) - \ln(|\mathbf{W}^{-1}|)), \quad (77)$$

where the unknown parameter is \mathbf{W} , the measurement covariance matrix. Then taking the derivative with respect to \mathbf{W}^{-1} we have

$$\frac{\partial V(q|\mathbf{W})}{\partial \mathbf{W}^{-1}} = \frac{1}{2} \sum_{k=1}^K \mathbb{E}_{q_k} [\mathbf{e}_k(\mathbf{x}_k) \mathbf{e}_k(\mathbf{x}_k)^T] - \frac{K}{2} \mathbf{W}. \quad (78)$$

Setting this to zero for a minimum we have

$$\mathbf{W} = \frac{1}{K} \sum_{k=1}^K \mathbb{E}_{q_k} [\mathbf{e}_k(\mathbf{x}_k) \mathbf{e}_k(\mathbf{x}_k)^T], \quad (79)$$

where we can use cubature to evaluate the marginal expectations. Reiterating, we never require the full covariance matrix, Σ , implying that our exactly sparse framework extends to parameter estimation.

6 Evaluation

We compared several variants of our algorithm on three different test problems: (i) a scalar toy problem motivated by a stereo camera to show that ESGVI achieves a better estimate than MAP, (ii) a multi-dimensional SLAM problem that shows we can carry out ESGVI in a tractable way, and (iii) a SLAM problem using a real robotics dataset that shows the new methods work well in practice.

Table 2 lists the variants of ESGVI that we studied as well as two MAP variants for comparison. The methods differ in the way the expectations of (47) are evaluated. ‘Analytical’ means that we calculate derivatives in closed form whereas

‘derivative-free’ means we used Stein’s lemma to avoid derivatives. All the methods attempt to minimize $V(q)$ (i.e., they are running our Newton-style optimizer) unless they have the ‘GN’ (Gauss-Newton) designation, which indicates that they are using the alternate loss functional, $V'(q)$, from Section 5.1. All the methods use cubature to calculate the expectations, but the number of points per dimension is varied. The MAP methods are simply special cases of the ESGVI approach in which we use analytical derivatives and a single quadrature point located at the mean of the current estimate.

All the methods use the ‘plain vanilla’ optimization scheme exactly as described in the paper with the exception of one extra feature. When updating the mean and inverse covariance, we allow backtracking if the loss functional is not reduced. In other words, we attempt to update according to

$$\boldsymbol{\mu}^{(i+1)} \leftarrow \boldsymbol{\mu}^{(i)} + \alpha^B \delta \boldsymbol{\mu}, \quad (80a)$$

$$\Sigma^{-1(i+1)} \leftarrow \Sigma^{-1(i)} + \alpha^B \delta \Sigma^{-1}, \quad (80b)$$

where $\alpha = 0.95$ and with $B = 0, 1, 2, \dots$ increasing until the loss functional goes down from the previous iteration. All the methods tested were allowed to do this in the same way and used (48) to calculate the loss functional.

6.1 Experiment 1: Stereo One-Dimensional Simulation

Our first simulation is a simple one-dimensional, nonlinear estimation problem motivated by the type of inverse-distance nonlinearity found in a stereo camera model. As this problem is only one-dimensional, we cannot demonstrate the ability to exploit sparsity in the problem, leaving this to the next two subsections. Here our aim is to show that indeed our proposed iterative scheme converges to the minimum of our loss functional and also that we offer an improvement over the usual MAP approach.

This same experiment (with the same parameter settings) was used as a running example by Barfoot (2017, §4). We assume that our true state is drawn from a Gaussian prior:

$$x \sim \mathcal{N}(\mu_p, \sigma_p^2). \quad (81)$$

We then generate a measurement according to

$$y = \frac{fb}{x} + n, \quad n \sim \mathcal{N}(0, \sigma_r^2), \quad (82)$$

where n is measurement noise. The numerical values of the parameters used in our trials were

$$\begin{aligned} \mu_p &= 20 \text{ [m]}, & \sigma_p^2 &= 9 \text{ [m}^2\text{]}, \\ f &= 400 \text{ [pixel]}, & b &= 0.1 \text{ [m]}, & \sigma_r^2 &= 0.09 \text{ [pixel}^2\text{]}. \end{aligned} \quad (83)$$

The two factors are defined as

$$\phi = \frac{1}{2} \frac{(x - \mu_p)^2}{\sigma_p^2}, \quad \psi = \frac{1}{2} \frac{\left(y - \frac{fb}{x}\right)^2}{\sigma_r^2}, \quad (84)$$

so that $-\ln p(\mathbf{x}, \mathbf{z}) = \phi + \psi + \text{constant}$. Our loss functional is therefore

$$V(q) = \mathbb{E}_q[\phi] + \mathbb{E}_q[\psi] + \frac{1}{2} \ln(\sigma^{-2}), \quad (85)$$

where $q = \mathcal{N}(\mu, \sigma^2)$ is our estimate of the posterior. We seek to find the q to minimize $V(q)$. This problem can also be viewed as the correction step of the Bayes filter (Jazwinski 1970): start from a prior and correct it based on the latest (nonlinear) measurement.

To conduct a proper Bayesian experiment, we ran 100,000 trials where each one consisted of drawing the latent state from the prior, then producing a noisy measurement given that state. To stay clear of edge cases (e.g., negative distance), we only accepted a draw of the latent state if it was within 4 standard deviations of the mean, resulting in 6 out of the 100,000 experiments to not be accepted and the state redrawn. We then ran several variants of our algorithm summarized in Table 2. Everything else to do with the experiment was the same for all algorithms, allowing a fair comparison. Figure 1 shows the statistical results of our 100,000 trials as boxplots. The columns correspond to the different versions of our algorithm while the rows are different performance metrics. The first column (analytical Hessian and Jacobian with a single quadrature point at the mean) is equivalent to a standard MAP approach. We can see that our new algorithms do require a few more iterations (first row) to converge than MAP, which is to say that it takes more computation to arrive at a better approximation to the posterior. We also see that the new algorithms do find a lower final value of the loss functional, $V(q)$, which is what we asked them to minimize (second row).

We also wanted to see if the new algorithms were less biased and more consistent than MAP, and so calculated the bias as the sum of errors (third row), squared error (fourth row), and squared Mahalanobis / Normalized Estimation Squared Error (NEES) (fifth row). We cannot ask the estimator to minimize these quantities (because they are based on knowledge of the groundtruth values of the latent state) but our hypothesis has been that by minimizing $V(q)$, we should also do better on these metrics. Looking at the third row, all the GVI variants are less biased than MAP by an order of magnitude or more. Our MAP error of -30.6 cm is consistent with the result reported by Barfoot (2017, §4). The best algorithm reported there, the Iterated Sigmoid Kalman Filter (ISPKF) (Sibley et al. 2006), had a bias of -3.84 cm. Our best algorithm had a bias of 0.3 cm. Squared error (fourth row) is also slightly improved compared to MAP.

The squared Mahalanobis / NEES error should be close to 1 for a one-dimensional problem; here the results are mixed, with some of our approaches doing better than MAP and some not. It seems that our choice of $\text{KL}(q||p)$ rather than $\text{KL}(p||q)$ results in a slightly overconfident covariance. Bishop (2006, fig 10.1) shows a similar situation for the same choice of $\text{KL}(q||p)$ as does Ala-Luhtala et al. (2015). As discussed earlier, it may be possible to overcome this by changing the relative weighting between the two main terms in $V(q)$ through the use of a metaparameter that is optimized for a particular situation.

Figure 2 shows the details of a single trial of the 100,000 that we ran. We show only a subset of the algorithms (rows) in the interest of space. The left column provides a contour plot of $V(q)$ (μ on the horizontal and σ^{-2} on the vertical) and the path the optimizer actually took to arrive at its minimum (red dot) starting from the prior (green dot). The right column shows the value of $V(q)$ at each iteration. It is worth noting that we show the true value of the loss (calculated using (48) with a large number of quadrature points) as well as the approximation of the loss that the algorithm had access to during its iterations (each algorithm used a different number of quadrature points, M). We see that the MAP approach clearly does not terminate at the minimum of $V(q)$; its approximation of the required expectations is too severe to converge to the minimum. The other algorithms end up very close to the true minimum, in a similar number of iterations.

In the next section, we introduce time and allow our simulated robot to move along the x -axis, with the same nonlinear stereo camera model. Our aim is to show that we can exploit the sparse structure of the problem in higher dimensions. We deliberately chose a SLAM problem to showcase that our ESGVI approach can work even when the probabilistic graphical model has loops.

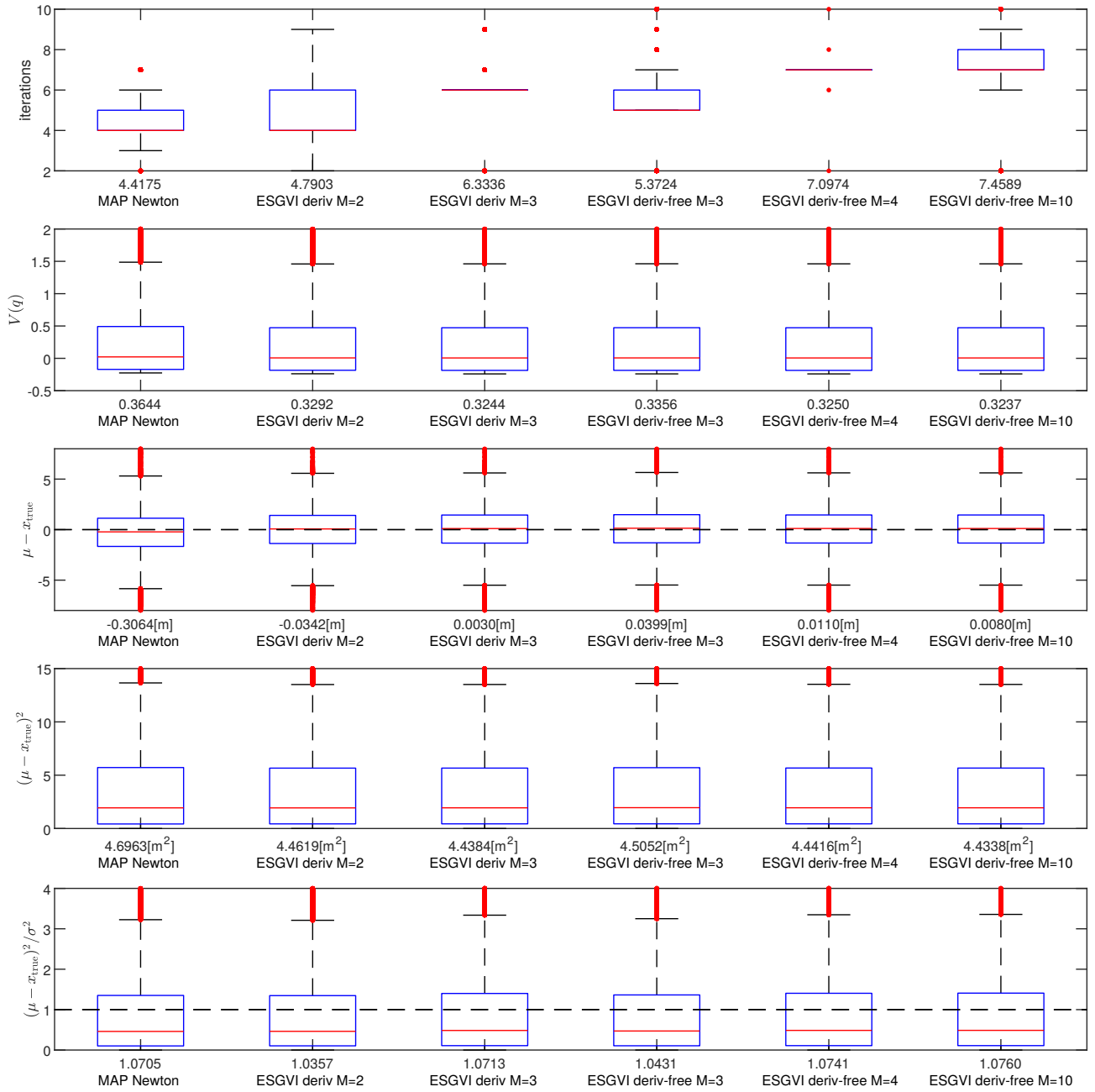


Figure 1. (Experiment 1) Statistical results of 100,000 trials of the one-dimensional stereo camera simulation shown as standard boxplots. The different rows show different performance metrics for the different variants of our algorithm (columns). Table 2 provides details of the different algorithms tested. The number above an algorithm label is its mean performance on that metric. Further details are discussed in the text.

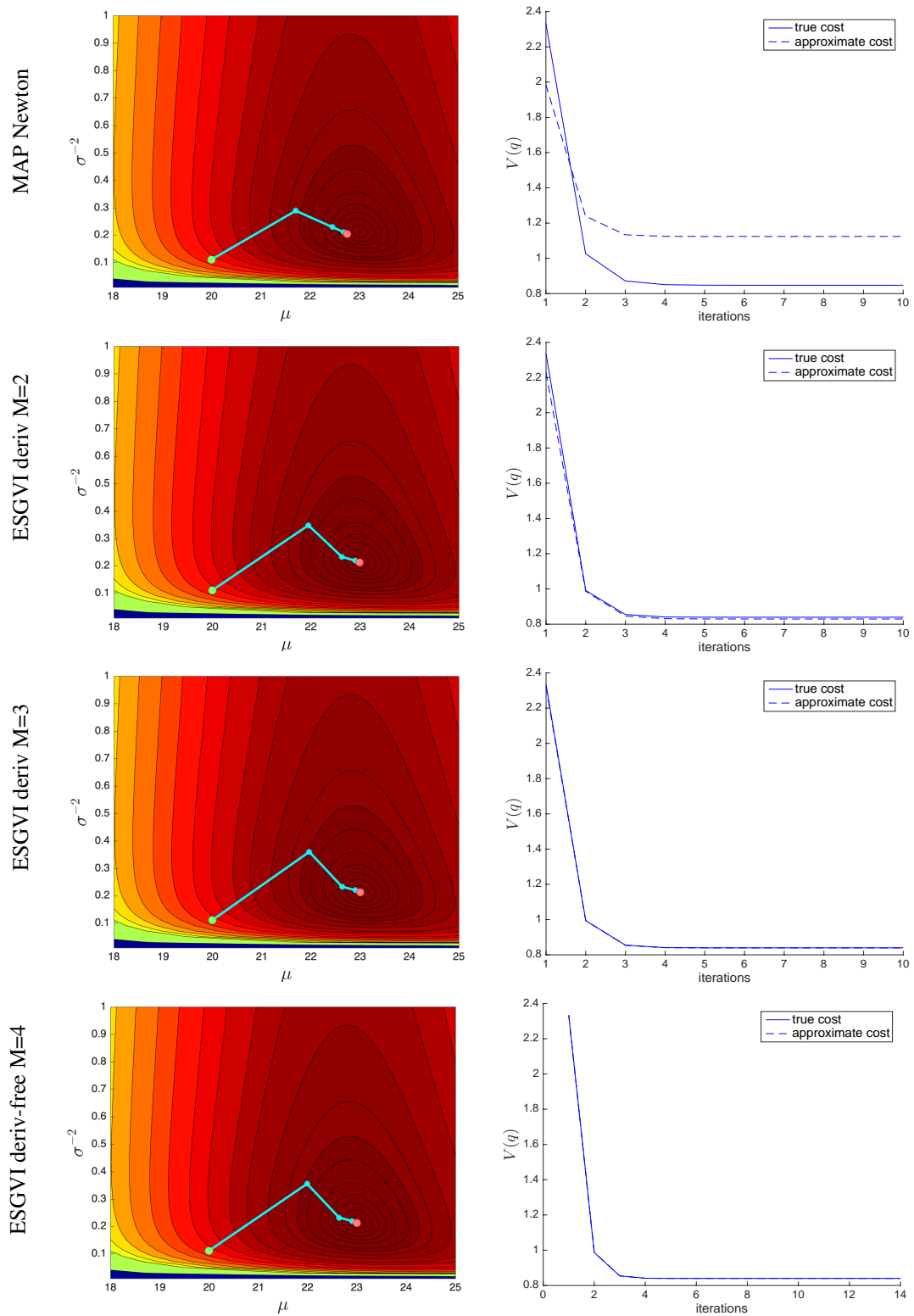


Figure 2. (Experiment 1) One trial of the one-dimensional stereo camera simulation showing the convergence history for four different algorithms shown in each row. The left column shows a contour map of the loss functional, $V(q)$, with the steps the optimizer took starting from the prior (green dot) to its converged value (red dot). The right column shows the loss at each iteration; as each algorithm makes different approximations to the loss during execution, we show the loss that each algorithm used to make decisions and the actual loss at each step.

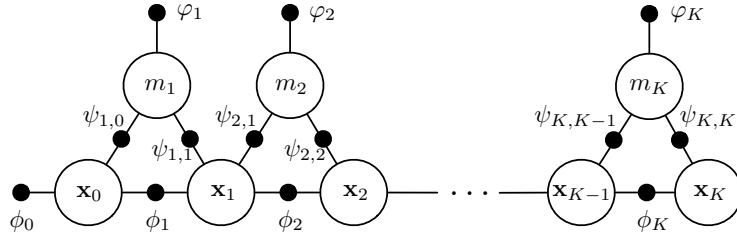


Figure 3. (Experiment 2) Factor graph for the stereo K -dimensional simulation. White circles represent variables to be estimated (both robot positions and landmark positions). Small black dots represent factors in the joint likelihood of the state and data.

6.2 Experiment 2: Stereo K -Dimensional Simulation

This simulation was designed to show that we can scale up to a more realistic problem size, while still deriving benefit from our variational approach. We extend the stereo camera problem from the previous section to the time domain by allowing a robot to move along the x -axis. In order to continue to carry out a proper Bayesian comparison of algorithms, we introduce a prior both on the robot motion and on the landmark positions in this SLAM problem. The *factor graph* for the problem can be seen in Figure 3.

The state to be estimated is

$$\mathbf{x} = \begin{bmatrix} \mathbf{x}_0 \\ \mathbf{x}_1 \\ \vdots \\ \mathbf{x}_K \\ m_1 \\ \vdots \\ m_K \end{bmatrix}, \quad \mathbf{z}_k = \begin{bmatrix} p_k \\ v_k \end{bmatrix}, \quad (86)$$

where p_k is a robot position, v_k a robot speed, and m_k a landmark position. The problem is highly structured as each landmark is seen exactly twice, from two consecutive robot positions.

For the (linear) prior factors we have

$$\phi_k = \begin{cases} \frac{1}{2}(\mathbf{x}_0 - \check{\mathbf{x}}_0)^T \check{\mathbf{P}}^{-1}(\mathbf{x}_0 - \check{\mathbf{x}}_0) & k = 0 \\ \frac{1}{2}(\mathbf{x}_k - \mathbf{A}\mathbf{x}_{k-1})^T \mathbf{Q}^{-1} \times (\mathbf{x}_k - \mathbf{A}\mathbf{x}_{k-1}) & k > 0 \end{cases}, \quad (87a)$$

$$\varphi_k = \frac{1}{2} \frac{(m_k - \mu_{m,k})^2}{\sigma_m^2}, \quad (87b)$$

with

$$\check{\mathbf{P}} = \text{diag}(\sigma_p^2, \sigma_v^2), \quad \mathbf{A} = \begin{bmatrix} 1 & T \\ 0 & 1 \end{bmatrix}, \quad \mathbf{Q} = \begin{bmatrix} \frac{1}{3}T^3 Q_C & \frac{1}{2}T^2 Q_C \\ \frac{1}{2}T^2 Q_C & T Q_C \end{bmatrix}, \quad (88)$$

where T is the discrete-time sampling period, Q_C is a power spectral density, and σ_p^2 , σ_v^2 , σ_m^2 are variances.

The robot state prior encourages constant velocity (Barfoot 2017, §3, p.85). The landmark prior is simply a Gaussian centered at the true landmark location, $\mu_{m,k}$.

For the (nonlinear) measurement factors we have

$$\psi_{\ell,k} = \frac{1}{2} \frac{\left(y_{\ell,k} - \frac{fb}{m_{\ell}-p_k}\right)^2}{\sigma_r^2}, \quad (89)$$

where f and b are the camera parameters (same as the previous experiment), $y_{\ell,k}$ is the disparity measurement of the ℓ th landmark from the k th position, and σ_r^2 is the measurement noise variance.

The negative log-likelihood of the state and data is then

$$-\ln p(\mathbf{x}, \mathbf{z}) = \sum_{k=0}^K \phi_k + \sum_{k=1}^K \varphi_k + \sum_{k=1}^K (\psi_{k,k-1} + \psi_{k,k}) + \text{constant}. \quad (90)$$

We set the maximum number of timesteps to be $K = 99$ for this problem, resulting in an overall state dimension of 299. Figure 4 shows the sparsity patterns of Σ^{-1} , \mathbf{L} , and the blocks of Σ that get computed by the method of Takahashi et al. (1973). This can very likely be improved further using modern sparsity techniques but the point is that we have a proof-of-concept scheme that can compute the subset of blocks of Σ required to carry out GVI.

We ran 10,000 trials of this simulation. In each trial, we drew the latent robot trajectory and landmark states from the Bayesian prior, then simulated the nonlinear measurements with a random draw of the noise. We estimated the full state using four different algorithms from Table 2: ‘MAP Newton’, ‘ESGVI deriv M=2’, ‘ESGVI deriv M=3’, and ‘ESGVI deriv-free M=4’.

Figure 5 shows the statistical results of the 10,000 trials. All the algorithms converge well in a small number of iterations (usually 4). Increasing the number of cubature points for the derivative-based methods does result in reducing the overall value of the loss functional, $V(q)$; the ‘ESGVI deriv-free M=4’ method does about as well as

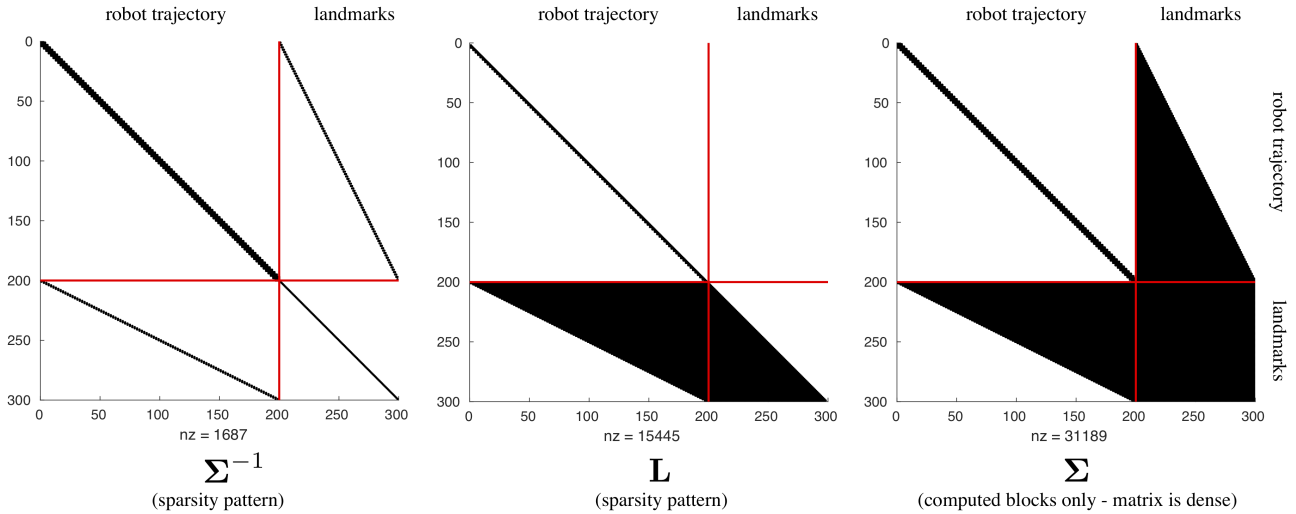


Figure 4. (Experiment 2) Sparsity patterns for the stereo K -dimensional simulation. The red partition lines separate the robot state variables from the landmark variables. The inverse covariance, Σ^{-1} , is highly sparse owing to the factor graph pattern in Figure 3; only $1,687/89,401 = 1.9\%$ of entries are nonzero. After performing a lower-diagonal-upper decomposition, the lower factor, L , becomes more filled in owing to the ‘four corners of a box’ rule; $15,445/89,401 = 17.3\%$ of entries are non-zero. Finally, we see that only a fraction of the entries of Σ are required despite the fact that this matrix is actually dense; since Σ is symmetric, we only need to calculate 17.3% of it as well.

Table 3. (Experiment 2) Wall-clock time per iteration for tested algorithms.

algorithm label	wall-clock time per iteration [s]
MAP Newton	0.0262
ESGVI deriv M=2	0.0745
ESGVI deriv M=3	0.1836
ESGVI deriv-free M=4	0.2653

the ‘ESGVI deriv M=3’ method but requires no analytical derivatives of the factors.

As in the one-dimensional simulation, the bias in the estimate is significantly reduced in the ESGVI approaches compared to the MAP approach (row 3 of Figure 5). This is important since this result can be achieved in a tractable way for large-scale problems and even without analytical derivatives. Note that we chose to show this metric separately for (left to right) robot position, robot velocity, and landmark position to avoid combining quantities with different units. We can see that the improvements offered by ESGVI are mostly due to the robot position variables but robot velocity and landmark positions are also improved.

The ESGVI methods also do slightly better than MAP on squared error (row 4 of Figure 5). Again, we chose to show this metric separately for (left to right) robot position, robot velocity, and landmark position to avoid combining quantities with different units. We can see that the improvements offered by ESGVI are mostly on the

robot position variables. For squared Mahalanobis distance / NEES (row 5 of Figure 5), all algorithms perform well.

Table 3 shows the wall-clock time per iteration for the different algorithms. Naturally, as we use more cubature points, the computational cost increases. The derivative-free version of ESGVI is about an order of magnitude slower than the MAP approach. We believe that there may be applications where this increased computational cost is worthwhile in terms of increased performance or the convenience of avoiding the calculation of derivatives.

6.3 Experiment 3: Robot Dataset

Finally, we consider a batch SLAM problem with a robot driving around and building a map of landmarks as depicted in Figure 6. The robot is equipped with a laser rangefinder and wheel odometers and must estimate its own trajectory and the locations of a number of tubular landmarks. This dataset has been used previously by Barfoot et al. (2014) to test SLAM algorithms. Groundtruth for both the robot trajectory and landmark positions (this is a unique aspect of this dataset) is provided by a Vicon motion capture system. The whole dataset is 12,000 timesteps long, which we broke into six subsequences of 2000 timestamps; statistical performance reported below is an average over these six subsequences. We assume that the data association (i.e., which measurement corresponds to which landmark) is known in this experiment to restrict testing to the state estimation part of the problem.

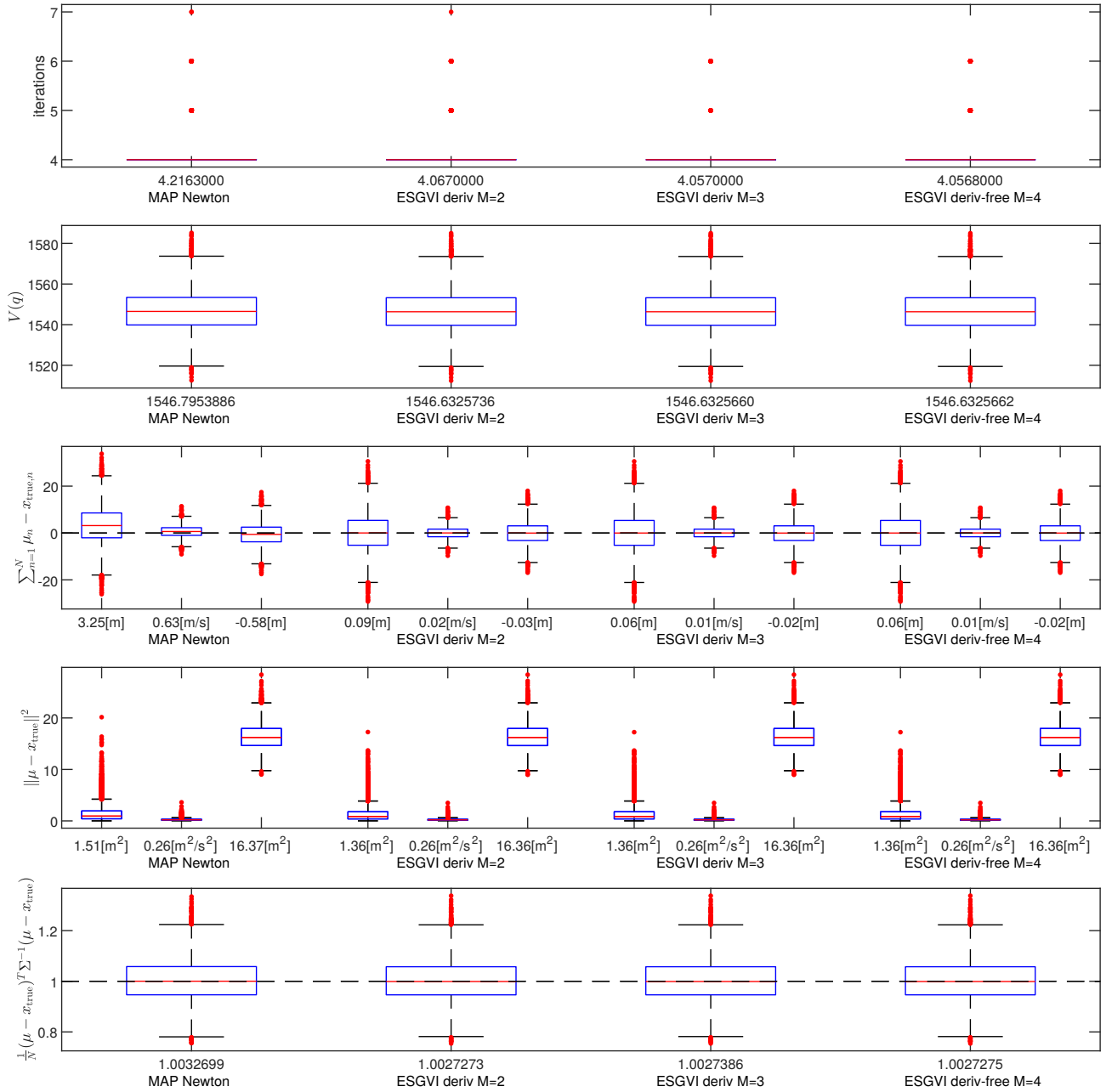


Figure 5. (Experiment 2) Statistical results of 10,000 trials of the K -dimensional stereo camera simulation shown as standard boxplots. The different rows show different performance metrics for the different variants of our algorithm (columns). Table 2 provides details of the different algorithms tested. For the bias (row 3) and squared error (row 4) metrics, we show the results separately for (left to right) robot position, robot velocity, and landmark position to avoid combining quantities with different units. The number above an algorithm label is its mean performance on that metric. Further details are discussed in the text.

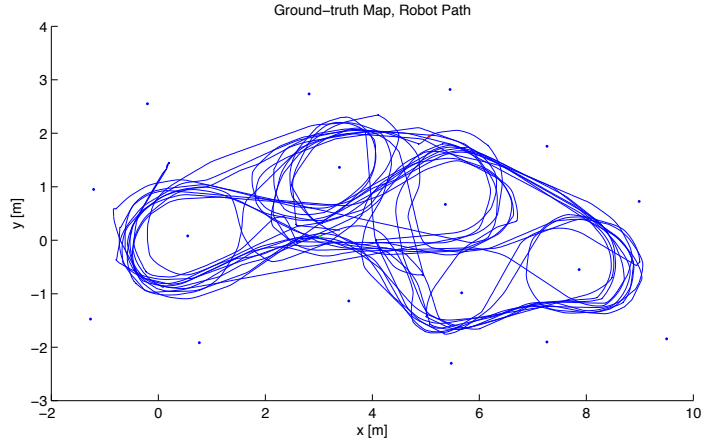


Figure 6. (Experiment 3) Setup: (left) a mobile robot navigates amongst a map of landmarks; it receives bearing measurements to some landmarks as well as wheel odometry. (right) the ground-truth path of the robot and landmark map as measured by an overhead camera system.

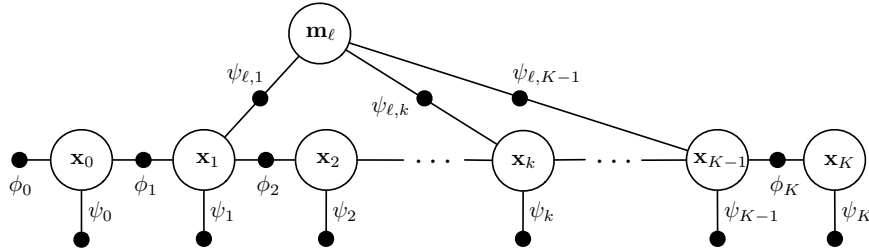


Figure 7. (Experiment 3) Factor graph for our robot dataset. White circles indicate variables and small black circles indicate factors involving variables.

The state to be estimated is

with

$$\mathbf{x} = \begin{bmatrix} \mathbf{x}_0 \\ \mathbf{x}_1 \\ \vdots \\ \mathbf{x}_K \\ \mathbf{m}_1 \\ \vdots \\ \mathbf{m}_L \end{bmatrix}, \quad \mathbf{x}_k = \begin{bmatrix} x_k \\ y_k \\ \theta_k \\ \dot{x}_k \\ \dot{y}_k \\ \dot{\theta}_k \end{bmatrix}, \quad \mathbf{m}_\ell = \begin{bmatrix} x_\ell \\ y_\ell \end{bmatrix}, \quad (91)$$

$$\begin{aligned} \check{\mathbf{P}} &= \text{diag}(\sigma_x^2, \sigma_y^2, \sigma_\theta^2, \sigma_{\dot{x}}^2, \sigma_{\dot{y}}^2, \sigma_{\dot{\theta}}^2), \quad \mathbf{A} = \begin{bmatrix} \mathbf{1} & T\mathbf{1} \\ \mathbf{0} & \mathbf{1} \end{bmatrix}, \\ \mathbf{Q} &= \begin{bmatrix} \frac{1}{3}T^3\mathbf{Q}_C & \frac{1}{2}T^2\mathbf{Q}_C \\ \frac{1}{2}T^2\mathbf{Q}_C & T\mathbf{Q}_C \end{bmatrix}, \\ \mathbf{Q}_C &= \text{diag}(Q_{C,1}, Q_{C,2}, Q_{C,3}), \end{aligned} \quad (93)$$

where \mathbf{x}_k is a robot state and \mathbf{m}_ℓ a landmark position. For each of our six subsequences we have $K = 2000$ and $L = 17$.

Figure 7 shows the factor graph for this experiment and Figure 8 shows the corresponding sparsity patterns. For the (linear) prior factor on the robot states we have

$$\phi_k = \begin{cases} \frac{1}{2}(\mathbf{x}_0 - \check{\mathbf{x}}_0)^T \check{\mathbf{P}}^{-1}(\mathbf{x}_0 - \check{\mathbf{x}}_0) & k = 0 \\ \frac{1}{2}(\mathbf{x}_k - \mathbf{A}\mathbf{x}_{k-1})^T \mathbf{Q}^{-1}(\mathbf{x}_k - \mathbf{A}\mathbf{x}_{k-1}) & k > 0 \end{cases}, \quad (92)$$

where T is the discrete-time sampling period, $Q_{C,i}$ are power spectral densities, and $\sigma_x^2, \sigma_y^2, \sigma_\theta^2, \sigma_{\dot{x}}^2, \sigma_{\dot{y}}^2, \sigma_{\dot{\theta}}^2$ are variances. The robot state prior encourages constant velocity (Barfoot 2017, §3, p.85). Unlike the previous experiment, we do not have a prior on the landmark positions; this was necessary when conducting a proper Bayesian evaluation in the previous experiment, but here we simply have a standard SLAM problem.

The (nonlinear) odometry factors, derived from wheel encoder measurements, are

$$\psi_k = \frac{1}{2}(\mathbf{v}_k - \mathbf{C}_k\mathbf{x}_k)^T \mathbf{S}^{-1}(\mathbf{v}_k - \mathbf{C}_k\mathbf{x}_k), \quad (94)$$

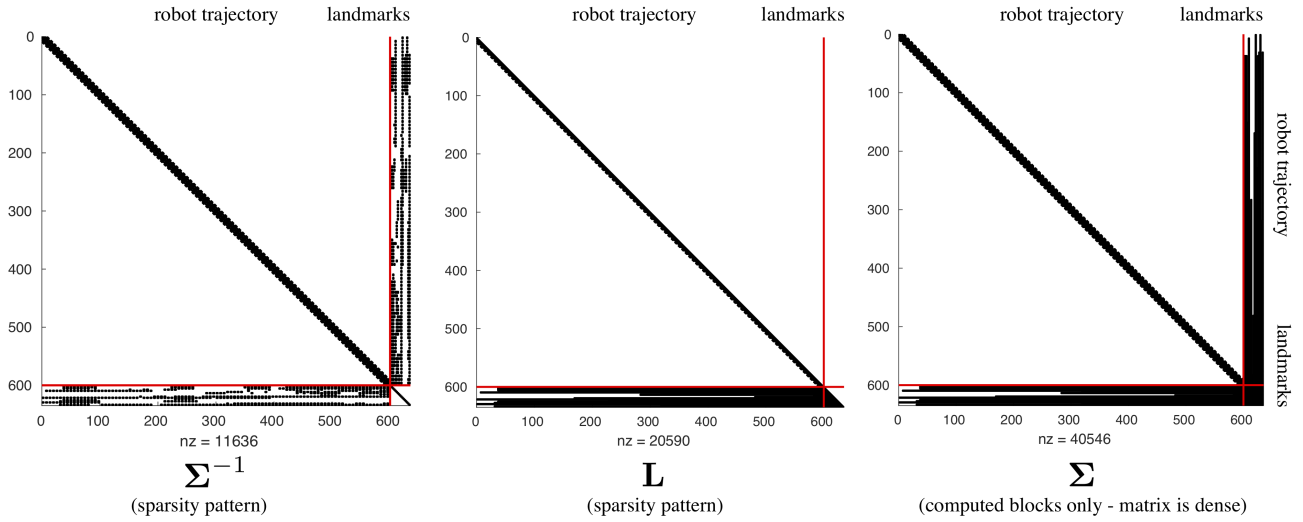


Figure 8. (Experiment 3) Sparsity patterns for the first 100 of 2000 timestamps of the robot dataset. The red partition lines separate the robot state variables from the landmark variables. The inverse covariance, Σ^{-1} , is highly sparse owing to the factor graph pattern in Figure 7; only $11,636/401,956 = 2.9\%$ of entries are nonzero. After performing a lower-diagonal-upper decomposition, the lower factor, L , becomes more filled in owing to the ‘four corners of a box’ rule; $20,590/401,956 = 5.1\%$ of entries are non-zero. Finally, we see that only a fraction of the entries of Σ are required despite the fact that this matrix is actually dense; since Σ is symmetric, we only need to calculate 5.1% of it as well. For the full 2000-timestamp dataset the sparsity is even more favourable for ESGVI, but the landmark part of the pattern becomes difficult to visualize due to its small size relative to the trajectory part.

where

$$\mathbf{v}_k = \begin{bmatrix} u_k \\ v_k \\ \omega_k \end{bmatrix}, \quad \mathbf{C}_k = \begin{bmatrix} 0 & 0 & 0 & \cos \theta_k & \sin \theta_k & 0 \\ 0 & 0 & 0 & -\sin \theta_k & \cos \theta_k & 0 \\ 0 & 0 & 0 & 0 & 0 & 1 \end{bmatrix},$$

$$\mathbf{S} = \text{diag}(\sigma_u^2, \sigma_v^2, \sigma_\omega^2). \quad (95)$$

The \mathbf{v}_k consists of measured forward, lateral, and rotational speeds in the robot frame, derived from wheel encoders; we set $v_k = 0$, which enforces the nonholonomy of the wheels as a soft constraint. The σ_u^2 , σ_v^2 , and σ_ω^2 are measurement noise variances.

The (nonlinear) bearing measurement factors, derived from a laser rangefinder, are

$$\psi_{\ell,k} = \frac{1}{2} \frac{(\beta_{\ell,k} - g(\mathbf{m}_\ell, \mathbf{x}_k))^2}{\sigma_r^2}, \quad (96)$$

with

$$g(\mathbf{m}_\ell, \mathbf{x}_k) = \text{atan2}(y_\ell - y_k - d \sin \theta_k, x_\ell - x_k - d \cos \theta_k) - \theta_k, \quad (97)$$

where $\beta_{\ell,k}$ is a bearing measurement from the k th robot pose to the ℓ th landmark, d is the offset of the laser rangefinder from the robot center in the longitudinal direction, and σ_r^2 is measurement noise variance. Although the dataset provides range to the landmarks as well, we chose to neglect these measurements to accentuate the

differences between the various algorithms. Our setup is similar to a monocular camera situation, which is known to be a challenging SLAM problem.

Putting these together, our joint state/data likelihood in this case is of the form

$$-\ln p(\mathbf{x}, \mathbf{z}) = \sum_{k=0}^K \phi_k + \sum_{k=0}^K \psi_k + \sum_{k=1}^K \sum_{\ell=1}^L \psi_{\ell,k} + \text{constant}, \quad (98)$$

where it is understood that not all $L = 17$ landmarks are actually seen at each timestep and thus we must remove the factors for unseen landmarks.

By using only bearing measurements, this proved to be a challenging dataset. We initialized our landmark locations using the bearing-only Random Sample And Consensus (RANSAC) (Fischler and Bolles 1981) strategy described by McGarey et al. (2017). We attempted to initialize our robot states using only the wheel odometry information, but this proved too difficult for methods making use of the full Hessian (i.e., Newton’s method). To remedy this problem, we used wheel odometry to initialize Gauss-Newton and then used this to initialize Newton’s method. Specifically, we used MAP Gauss-Newton to initialize MAP Newton and ESGVI-GN to initialize ESGVI. To compare our results to groundtruth, we aligned the resulting landmark map to the groundtruth map since it is well established that SLAM

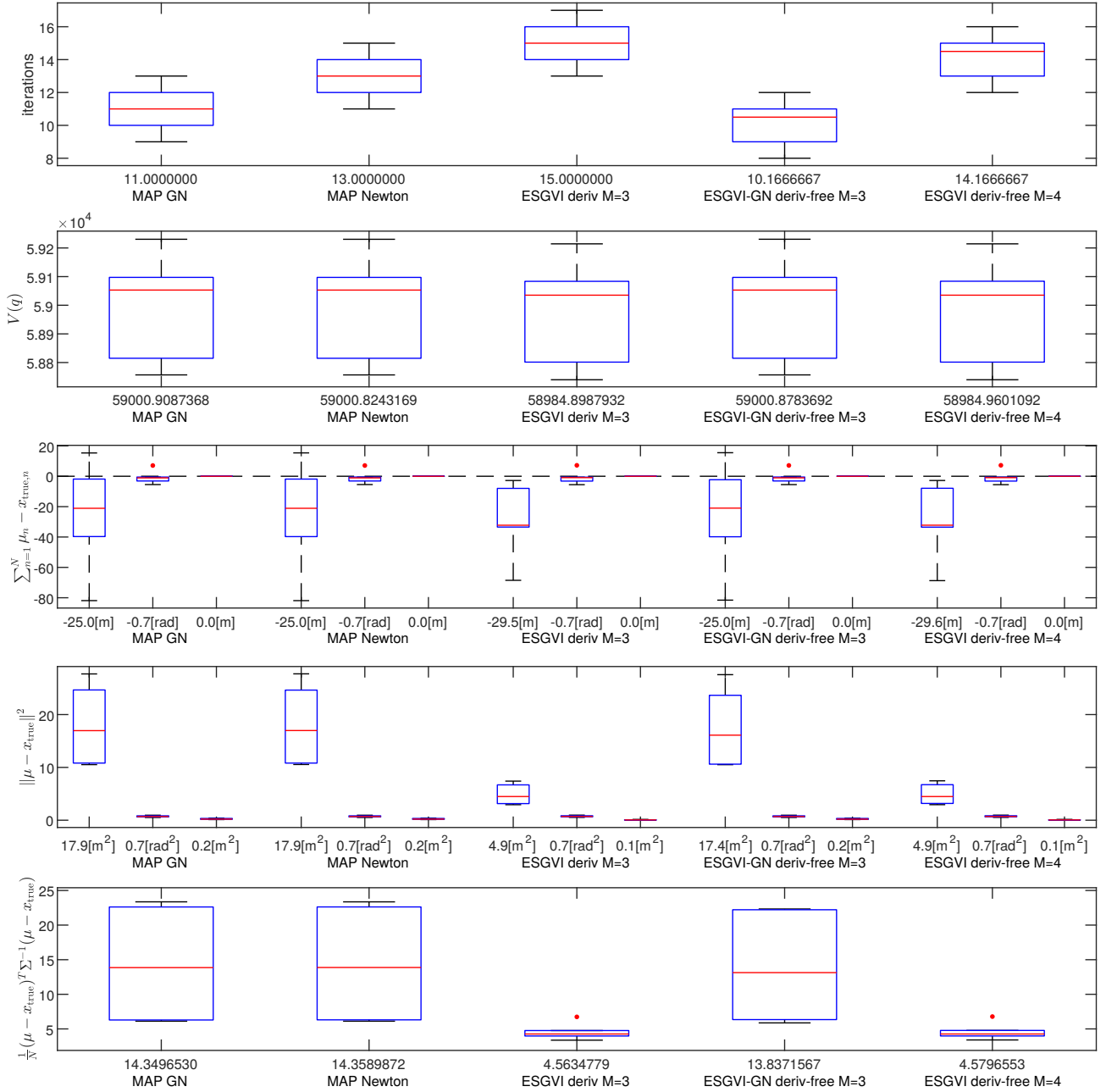


Figure 9. (Experiment 3) Statistical results of robot dataset shown as standard boxplots. The different rows show different performance metrics for the different variants of our algorithm (columns). Table 2 provides details of the different algorithms tested. For the bias (row 3) and squared error (row 4) metrics, we show the results separately for (left to right) robot position, robot orientation, and landmark position to avoid combining quantities with different units. The number above an algorithm label is its mean performance on that metric, averaged over all 2000 timestamps and six subsequences. Further details are discussed in the text.

Table 4. (Experiment 3) Wall-clock time per iteration for tested algorithms (averages over the 6 sequences).

algorithm label	wall-clock time per iteration [s]
MAP Newton	5.8079
MAP GN	1.2035
ESGVI deriv M=3	80.2644
ESGVI-GN deriv-free M=3	41.4672
ESGVI deriv-free M=4	164.0719

produces a relative solution; reported errors are calculated after this alignment.

Figure 9 provides the statistical results of several variants of our ESGVI algorithms. We see that the number of iterations required to converge is higher than in the previous experiments, with the ESGVI variants requiring a few more than the corresponding MAP algorithms. Again, we see the ESGVI variants reducing the loss functional, $V(q)$, further than the MAP methods.

The bias is further away from zero for the derivative-free ESGVI method than MAP, which could simply be related to the relatively small number of trials compared to the previous two experiments. Note, as in the previous experiment, we show the bias separately for (left to right) robot position, robot orientation, and landmark position to avoid combining quantities with different units. We do not have groundtruth for velocity so do not report errors for this part of the state.

The squared error and squared Mahalanobis distance metrics are drastically improved for the full ESGVI methods compared to the MAP method and even the ESGVI-GN method. Again, we show the squared error separately for (left to right) robot position, robot orientation, and landmark position to avoid combining quantities with different units. We can see that the improvements offered by ESGVI on squared error are due to the robot and landmark position variables rather than robot orientation.

Figure 10 shows the detailed error plots for one of the six subsequences for the ‘MAP GN’ and ‘ESGVI deriv-free M=4’ algorithms. The ESGVI path is visibly better than MAP in most sections. MAP seems to have underestimated the scale of the whole solution, resulting in much worse performance on all translational variables, while performing similarly on heading error. Both algorithms are fairly consistent, with ESGVI being both more confident and more consistent. The other five subsequences have similar results.

Figure 8 shows the sparsity patterns of Σ^{-1} and \mathbf{L} , as well as the blocks of Σ that are computed (the matrix is actually dense); only the patterns for the first 100 timestamps are shown for clarity, but each subsequence is actually 2000 timestamps long. In terms of computational

complexity, all of the algorithms for this SLAM problem are $O(L^3 + L^2K)$ per iteration, where L is the number of landmarks and K is the number of timesteps. However, the wall-clock time required by the different algorithms varies significantly due to different numbers of iterations and the accuracy with which the required expectations in (47) are computed. Table 4 reports how long each algorithm took per iteration; the ESGVI methods come at a cost, but this may be acceptable for batch (i.e., offline) applications. It is also worth noting that we have made little attempt to optimize our implementation. We used a brute-force cubature method requiring M^{N_k} sigmapoints where N_k is the number of state variables involved in a factor. More efficient options could be swapped in to speed up the evaluation of each factor. Additionally, parallelization could be employed at the factor level quite easily in our approach by evaluating the expectations in (47) in parallel across several compute elements.

7 Conclusion and Future Work

We presented our Exactly Sparse Gaussian Variational Inference (ESGVI) approach and demonstrated that it is possible to compute a Gaussian that is ‘best’ in terms of KL divergence from the full Bayesian posterior, even for large-scale problems. We exploited the fact that the joint likelihood of the state and data factors, a property of most common robotics problems, to show that the full (dense) covariance matrix is not required, only the blocks corresponding to the non-zero blocks of the (sparse) inverse covariance matrix. We further showed how to apply cubature methods (e.g., sigmapoints) within our framework resulting in a batch inference scheme that does not require analytical derivatives, yet is applicable to large-scale problems. The methods offer performance improvements (over MAP) that increase as the problem becomes more nonlinear and/or the posterior less concentrated.

There are several avenues for further exploration beyond this work. First, sample-efficient cubature methods could bring the cost of our scheme down further. While we showed that we only need to apply cubature at the factor/marginal level, this can still be expensive for marginals involving several state variables. We used a brute-force approach requiring M^{N_k} samples for a marginal of dimension N_k , but there may be other alternatives that could be applied to bring the cost down. Parallel evaluation of the factor expectations could also be worth investigating.

We used the method of Takahashi et al. (1973) to compute the blocks of Σ corresponding to the non-zero blocks of Σ^{-1} , but this basic method is not always optimally efficient, requiring additional (unnecessary) blocks of Σ to be computed for some GVI problems. It should be possible to combine this with additional modern sparsity methods such as variable reordering and Givens

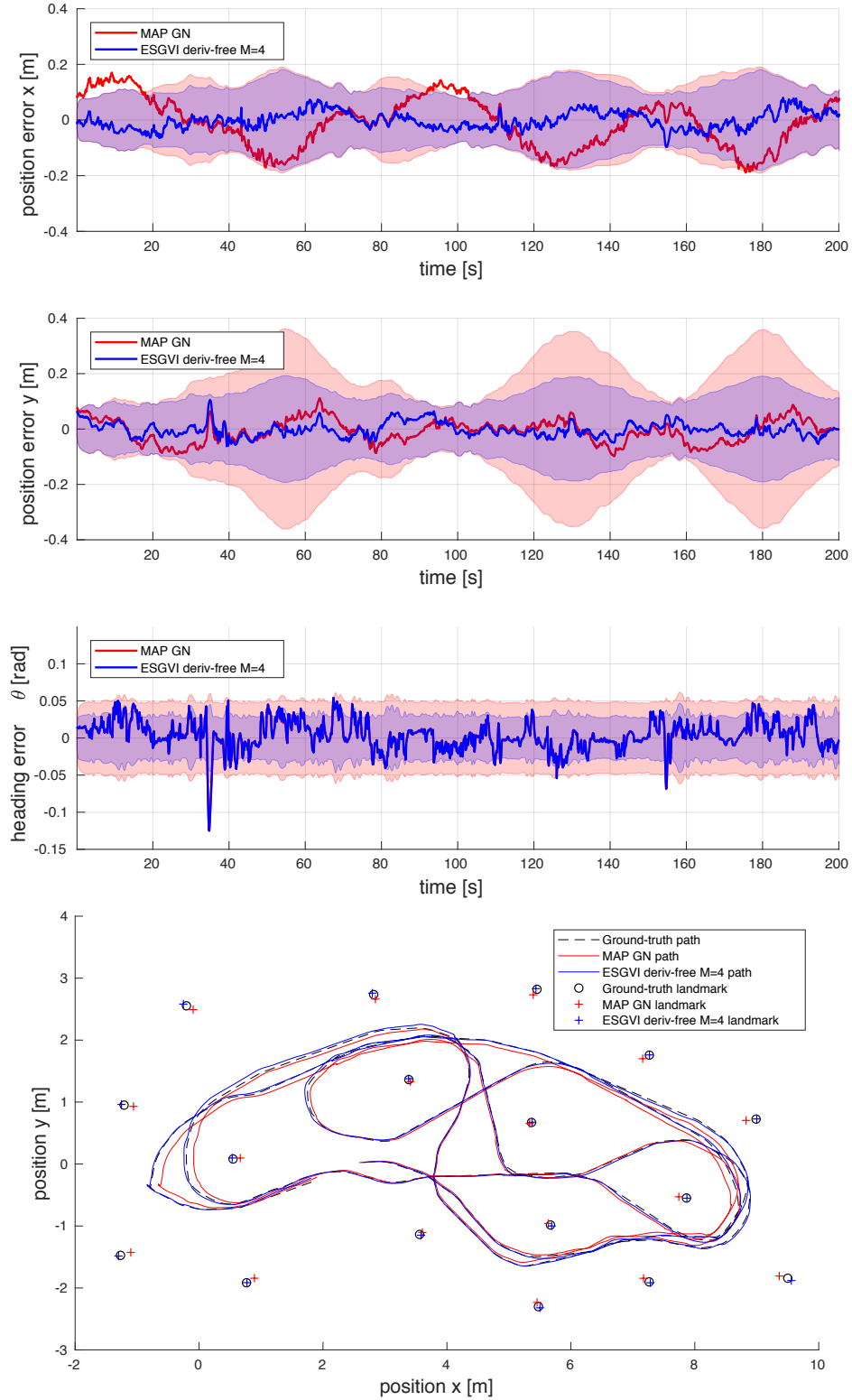


Figure 10. (Experiment 3) A comparison of ‘MAP GN’ and ‘ESGVI deriv-free M=4’ on one of the six subsequences of 2000 timestamps. Above, we see the individual error plots (with 3σ covariance envelopes) for the x , y , and θ components of the robot state as compared to groundtruth. Below, we have an overhead view of the robot path and landmark map for the two algorithms as well as groundtruth. The total landmark squared error for ‘MAP GN’ was $0.2214 \text{ [m}^2\text{]}$ while for ‘ESGVI deriv-free M=4’ it was $0.0168 \text{ [m}^2\text{]}$.

rotations (Golub and Van Loan 1996; Kaess et al. 2008) to improve the efficiency of this step.

Our SLAM experiments showed that we could carry out GVI in a tractable manner. However, we have not yet shown that our approach is robust to outliers. It would certainly be worth attempting to wrap each factor expression in a robust cost function to enable a variational extension of M-estimation (Barfoot 2017, §5, p. 163)(MacTavish and Barfoot 2015). This is typically implemented as iteratively reweighted least squares (Holland and Welsch 1977), but ESGVI might handle robust cost functions with no modification since we compute expectations at the factor level.

There are many other practical applications of ESGVI worth exploring beyond the simple cases presented here. We are particularly interested in how to apply our inference approach to joint estimation-control problems and have begun an investigation along this line.

We restricted our variational estimate to be a single multivariate Gaussian, but the ideas here will likely extend to mixtures of Gaussians and possibly other approximations of the posterior as well. We have not explored this possibility yet, but the variational approach seems to offer a logical avenue along which to do so.

Finally, we showed the possibility of extending ESGVI to include parameter estimation through the use of an EM setup, which typically employs the same loss functional, $V(q|\theta)$. In particular, we would like to represent our factor models as Deep Neural Networks (DNNs) whose weights are unknown. We believe that ESGVI offers a good option for the expectation step, as we may be able to use our derivative-free version to avoid the need to take the derivative of a DNN with respect to the state being estimated, instead just carrying out hardware-accelerated feed-forward evaluations.

Acknowledgements

We are grateful to Filip Tronarp (Aalto University) as well as Paul Furgale, Colin McManus, and Chi Hay Tong (while they were at the University of Toronto) for some early discussions on this work. This work was supported by the Natural Sciences and Engineering Research Council of Canada.

References

- Abdulle A and Wanner G (2002) 200 years of least squares method. *Elemente der Mathematik* 57: 45–60.
- Ala-Luhtala J, Särkkä S and Piché R (2015) Gaussian filtering and variational approximations for bayesian smoothing in continuous-discrete stochastic dynamic systems. *Signal Processing* 111: 124–136.
- Amari SI (1998) Natural gradient works efficiently in learning. *Neural computation* 10(2): 251–276.
- Anderson S, Barfoot TD, Tong CH and Sarkka S (2015) Batch nonlinear continuous-time trajectory estimation as exactly sparse gaussian process regression. *Autonomous Robots* 39(3): 221–238.
- Arasaratnam I and Haykin S (2009) Cubature kalman filters. *IEEE Transactions on Automatic Control* 54(6): 1254–1269.
- Barfoot TD (2017) *State Estimation for Robotics*. Cambridge University Press.
- Barfoot TD (2020) Multivariate gaussian variational inference by natural gradient descent. Technical report, Autonomous Space Robotics Lab, University of Toronto. arXiv:2001.10025 [stat.ML].
- Barfoot TD, Tong CH and Sarkka S (2014) Batch continuous-time trajectory estimation as exactly sparse gaussian process regression. In: *Proceedings of Robotics: Science and Systems (RSS)*. Berkeley, USA.
- Bayes T (1764) Essay towards solving a problem in the doctrine of chances. *Philosophical Transactions of the Royal Society of London*.
- Bishop CM (2006) *Pattern Recognition and Machine Learning*. Springer.
- Bjorck A (1996) *Numerical Methods for Least Squares Problems*. Society for Industrial and Applied Mathematics (SIAM).
- Bourmaud G (2016) Online variational bayesian motion averaging. In: *Proceedings of the European Conference on Computer Vision (ECCV)*. pp. 126–142.
- Broussolle F (1978) State estimation in power systems: detecting bad data through the sparse inverse matrix method. *IEEE Transactions on Power Apparatus and Systems* (3): 678–682.
- Brown DC (1958) A solution to the general problem of multiple station analytical stereotriangulation. RCA-MTP Data Reduction Technical Report No. 43 (or AFMTC TR 58-8), Patrick Airforce Base, Florida.
- Cools R (1997) Constructing cubature formulae: The science behind the art. *Acta Numerica* 6: 1–54.
- Davison AJ and Ortiz J (2019) Futuremapping 2: Gaussian belief propagation for spatial ai.
- Dong J, Mukadam M, Dellaert F and Boots B (2016) Motion planning as probabilistic inference using gaussian processes and factor graphs. In: *Robotics: Science and Systems*, volume 12. p. 4.
- Durrant-Whyte H and Bailey T (2006) Simultaneous localisation and mapping (SLAM): Part I the essential algorithms. *IEEE Robotics and Automation Magazine* 11(3): 99–110.
- Erismann AM and Tinney WF (1975) On computing certain elements of the inverse of a sparse matrix. *Communications of the ACM* 18(3): 177–179.
- Fischler M and Bolles R (1981) Random sample consensus: a paradigm for model fitting with applications to image analysis and automated cartography. *Communications of ACM* 24(6): 381–395.

- Fisher RA (1922) On the mathematical foundations of theoretical statistics. *Philosophical Transactions of the Royal Society of London. Series A, Containing Papers of a Mathematical or Physical Character* 222(594-604): 309–368.
- García-Fernández ÁF, Svensson L, Morelande MR and Särkkä S (2015) Posterior linearization filter: Principles and implementation using sigma points. *IEEE transactions on signal processing* 63(20): 5561–5573.
- Gašperin M and Juričić D (2011) Application of unscented transformation in nonlinear system identification. *IFAC Proceedings Volumes* 44(1): 4428–4433.
- Gauss C (1809) *Theoria motus corporum coelestium, perthes et besser, hamburgi* 7.
- Gauss C (1821) *Theoria combinationis observationum erroribus minimis obnoxiae, pars prior. Werke, IV, Koniglichen Gesellschaft der Wissenschaften zu Gottingen* : 1–26.
- Gauss C (1823) *Theoria combinationis observationum erroribus minimis obnoxiae, pars posterior. Werke, IV, Koniglichen Gesellschaft der Wissenschaften zu Gottingen* : 27–53.
- Ghahramani Z and Roweis ST (1999) Learning nonlinear dynamical systems using an em algorithm. In: *Advances in neural information processing systems*. pp. 431–437.
- Golub H and Van Loan CF (1996) *Matrix computations*, Johns Hopkins uni. Press, London .
- Hoffman MD, Blei DM, Wang C and Paisley J (2013) Stochastic variational inference. *The Journal of Machine Learning Research* 14(1): 1303–1347.
- Holland PW and Welsch RE (1977) Robust regression using iteratively reweighted least-squares. *Communications in Statistics – Theory and Methods* 6(9): 813–827.
- Ito K and Xiong K (2000) Gaussian filters for nonlinear filtering problems. *IEEE Transactions on Automatic Control* 45(5): 910–927.
- Jazwinski AH (1970) *Stochastic Processes and Filtering Theory*. Academic, New York.
- Jensen JLWV (1906) Sur les fonctions convexes et les inégalités entre les valeurs moyennes. *Acta mathematica* 30: 175–193.
- Jia B, Xin M and Cheng Y (2013) High-degree cubature kalman filter. *Automatica* 49: 510–518.
- Julier S and Uhlmann J (1996) A general method for approximating nonlinear transformations of probability distributions. Technical report, Robotics Research Group, University of Oxford.
- Kaess M and Dellaert F (2009) Covariance recovery from a square root information matrix for data association. *Robotics and autonomous systems* 57(12): 1198–1210.
- Kaess M, Johannsson H, Roberts R, Ila V, Leonard J and Dellaert F (2011) isam2: Incremental smoothing and mapping with fluid relinearization and incremental variable reordering. In: *2011 IEEE International Conference on Robotics and Automation*. pp. 3281–3288.
- Kaess M, Ranganathan A and Dellaert F (2008) isam: Incremental smoothing and mapping. *IEEE Transactions on Robotics* 24(6): 1365–1378.
- Kalman RE (1960) A new approach to linear filtering and prediction problems. *Trans. ASME, Journal of Basic Engineering* 82: 35–45.
- Kokkala J, Solin A and Särkkä S (2014) Expectation maximization based parameter estimation by sigma-point and particle smoothing. In: *17th International Conference on Information Fusion (FUSION)*. IEEE, pp. 1–8.
- Kokkala J, Solin A and Särkkä S (2016) Sigma-point filtering and smoothing based parameter estimation in nonlinear dynamic systems. *Journal of Advances in Information Fusion* 11(1): 15–30.
- Kullback S and Leibler RA (1951) On information and sufficiency. *The annals of mathematical statistics* 22(1): 79–86.
- Li R, Hwangbo J, Chen Y and Di K (2011) Rigorous photogrammetric processing of HiRISE stereo imagery for mars topographic mapping. *IEEE Transactions on Geoscience and Remote Sensing* 49(7): 2558–2572.
- Lu F and Milios E (1997) Globally consistent range scan alignment for environment mapping. *Autonomous robots* 4(4): 333–349.
- MacTavish KA and Barfoot TD (2015) At all costs: A comparison of robust cost functions for camera correspondence outliers. In: *Proceedings of the 12th Conference on Computer and Robot Vision (CRV)*. Halifax, Canada, pp. 62–69. DOI: 10.1109/CRV.2015.52.
- Magnus JR and Neudecker H (2019) *Matrix differential calculus with applications in statistics and econometrics*. John Wiley & Sons.
- Markoff A (1912) *Wahrscheinlichkeitsrechnung*. Trans., Leipzig.
- McGarey P, MacTavish KA, Pomerleau F and Barfoot TD (2017) Tslam: Tethered simultaneous localization and mapping for mobile robots. *International Journal of Robotics Research (IJRR)* 36(12): 1363–1386. DOI:10.1177/0278364917732639.
- Meurant G (1992) A review on the inverse of symmetric tridiagonal and block tridiagonal matrices. *SIAM Journal of Matrix Analysis and Applications* 13(3): 707–728.
- Mukadam M, Dong J, Yan X, Dellaert F and Boots B (2018) Continuous-time gaussian process motion planning via probabilistic inference. *The International Journal of Robotics Research* 37(11): 1319–1340.
- Neal RM and Hinton GE (1998) A view of the em algorithm that justifies incremental, sparse, and other variants. In: *Learning in graphical models*. Springer, pp. 355–368.
- Nocedal J and Wright SJ (2006) *Numerical Optimization*. 2nd edition. Springer.
- O’Hagan A (1991) Bayes–hermite quadrature. *Journal of statistical planning and inference* 29(3): 245–260.

- Opper M and Archambeau C (2009) The variational gaussian approximation revisited. *Neural computation* 21(3): 786–792.
- Ortega J and Rheinboldt W (1970) *Iterative Solution of Nonlinear Equations in Several Variables*. Academic Press.
- Park E, Park SY and Choi KH (2009) Performance comparison of the batch filter based on the unscented transformation and other batch filters for satellite orbit determination. *Journal of Astronomy and Space Sciences* 26(1): 75–88.
- Pradeep V, Konolige K and Berger E (2014) Calibrating a multi-arm multi-sensor robot: A bundle adjustment approach. In: *Experimental robotics*. Springer, pp. 211–225.
- Press WH, Teukolsky SA, Vetterling WT and Flannery BP (2007) *Numerical Recipes: The Art of Scientific Computing*. Cambridge.
- Ranganathan A, Kaess M and Dellaert F (2007) Loopy sam. In: *Proceedings of Intl. Joint Conf. on Artificial Intelligence (IJCAI)*. pp. 2191–2196.
- Rasmussen CE and Williams CKI (2006) *Gaussian Processes for Machine Learning*. Cambridge, MA: MIT Press.
- Rauch HE, Tung F and Striebel CT (1965) Maximum likelihood estimates of linear dynamic systems. *AIAA Journal* 3(8): 1445–1450.
- Roh KM, Park SY, Park ES and Choi KH (2007) A batch filter based on the unscented transformation and its applications to attitude estimation. *Advances in the Astronautical Sciences* 127(1): 19–40.
- Särkkä S (2013) *Bayesian Filtering and Smoothing*. Cambridge University Press.
- Särkkä S, Hartikainen J, Svensson L and Sandblom F (2016) On the relation between gaussian process quadratures and sigma-point methods. *Journal of Advances in Information Fusion* 11(1): 31–46.
- Sarmavuori J and Särkkä S (2012) Fourier-hermite kalman filter. *IEEE Transactions on Automatic Control* 57(6): 1511–1515.
- Schön TB, Wills A and Ninness B (2011) System identification of nonlinear state-space models. *Automatica* 47(1): 39–49.
- Sibley G, Sukhatme G and Matthies L (2006) The iterated sigma point kalman filter with applications to long-range stereo. In: *Proceedings of Robotics: Science and Systems*. Philadelphia, USA.
- Stein CM (1981) Estimation of the mean of a multivariate normal distribution. *Annals of Statistics* 9(6): 1135–1151.
- Takahashi K, Fagan J and Chen MS (1973) A sparse bus impedance matrix and its application to short circuit study. In: *Proceedings of the PICA Conference*.
- Thrun S, Burgard W and Fox D (2006) *Probabilistic Robotics*. MIT Press.
- Thrun S, Liu Y, Koller D, Ng AY, Ghahramani Z and Durrant-Whyte H (2004) Simultaneous localization and mapping with sparse extended information filters. *The international journal of robotics research* 23(7-8): 693–716.
- Thrun S and Montemerlo M (2005) The GraphSLAM algorithm with applications to large-scale mapping of urban structures. *International Journal on Robotics Research* 25(5/6): 403–430.
- Triggs W, McLauchlan P, Hartley R and Fitzgibbon A (2000) Bundle adjustment: A modern synthesis. In: Triggs W, Zisserman A and Szeliski R (eds.) *Vision Algorithms: Theory and Practice*, LNCS. Springer Verlag, pp. 298–375.
- Walter MR, Eustice RM and Leonard JJ (2007) Exactly sparse extended information filters for feature-based slam. *The International Journal of Robotics Research* 26(4): 335–359.
- Wu Y, Hu D, Wu M and Hu X (2006) Gaussian filters for nonlinear filtering problems. *IEEE Transactions on Signal Processing* 54(8): 2910–2921.

A Definiteness of $\text{tr}(\mathbf{A}\mathbf{B}\mathbf{A}\mathbf{B})$

We used the fact that

$$\text{tr} \left(\Sigma^{(i)} \delta \Sigma^{-1} \Sigma^{(i)} \delta \Sigma^{-1} \right) \geq 0, \quad (99)$$

with equality if and only if $\delta \Sigma^{-1} = \mathbf{0}$ in our local convergence guarantee in (16). To show this, it is sufficient to show for \mathbf{A} real symmetric positive definite and \mathbf{B} real symmetric that

$$\text{tr}(\mathbf{A}\mathbf{B}\mathbf{A}\mathbf{B}) \geq 0, \quad (100)$$

with equality if and only if $\mathbf{B} = \mathbf{0}$.

We can write

$$\begin{aligned} \text{tr}(\mathbf{A}\mathbf{B}\mathbf{A}\mathbf{B}) &= \text{vec}(\mathbf{A}\mathbf{B}\mathbf{A})^T \text{vec}(\mathbf{B}) \\ &= \text{vec}(\mathbf{B})^T \underbrace{(\mathbf{A} \otimes \mathbf{A})}_{>0} \text{vec}(\mathbf{B}) \geq 0, \end{aligned} \quad (101)$$

using basic properties of $\text{vec}(\cdot)$ and the Kronecker product, \otimes . The matrix in the middle is symmetric positive definite owing to our assumptions on \mathbf{A} . Therefore the quadratic form is positive semi-definite with equality if and only if $\text{vec}(\mathbf{B}) = \mathbf{0}$ if and only if $\mathbf{B} = \mathbf{0}$.

B Fisher Information Matrix for a Multivariate Gaussian

This section provides a brief derivation for the Fisher Information Matrix (FIM) associated with our Gaussian, $q = \mathcal{N}(\boldsymbol{\mu}, \Sigma)$. Magnus and Neudecker (2019) or Barfoot (2020) provide more detail. If we stack up our variational parameters into a vector as

$$\boldsymbol{\alpha} = \begin{bmatrix} \boldsymbol{\mu} \\ \text{vec}(\Sigma^{-1}) \end{bmatrix}, \quad (102)$$

then we seek to show that the FIM is

$$\mathcal{I}_{\boldsymbol{\alpha}} = \begin{bmatrix} \mathcal{I}_{\boldsymbol{\mu}} & \mathbf{0} \\ \mathbf{0} & \mathcal{I}_{\Sigma^{-1}} \end{bmatrix} = \begin{bmatrix} \Sigma^{-1} & \mathbf{0} \\ \mathbf{0} & \frac{1}{2}(\Sigma \otimes \Sigma) \end{bmatrix}. \quad (103)$$

For a Gaussian, we can use the following FIM definition (Fisher 1922):

$$\mathcal{I}_\alpha = -\mathbb{E}_q \left[\frac{\partial^2 \ln q}{\partial \alpha^T \partial \alpha} \right]. \quad (104)$$

The negative log-likelihood of a Gaussian is

$$-\ln q = \frac{1}{2}(\mathbf{x} - \boldsymbol{\mu})^T \boldsymbol{\Sigma}^{-1}(\mathbf{x} - \boldsymbol{\mu}) - \frac{1}{2} \ln |\boldsymbol{\Sigma}^{-1}| + \text{constant}. \quad (105)$$

The first differential is

$$-d \ln q = -d\boldsymbol{\mu}^T \boldsymbol{\Sigma}^{-1}(\mathbf{x} - \boldsymbol{\mu}) - \frac{1}{2} \text{tr}(\boldsymbol{\Sigma} d\boldsymbol{\Sigma}^{-1}) + \frac{1}{2}(\mathbf{x} - \boldsymbol{\mu})^T d\boldsymbol{\Sigma}^{-1}(\mathbf{x} - \boldsymbol{\mu}). \quad (106)$$

The second differential is

$$-d^2 \ln q = d\boldsymbol{\mu}^T \boldsymbol{\Sigma}^{-1} d\boldsymbol{\mu} - 2d\boldsymbol{\mu}^T d\boldsymbol{\Sigma}^{-1}(\mathbf{x} - \boldsymbol{\mu}) + \frac{1}{2} \text{tr}(((\mathbf{x} - \boldsymbol{\mu})(\mathbf{x} - \boldsymbol{\mu})^T - \boldsymbol{\Sigma}) d^2 \boldsymbol{\Sigma}^{-1}) + \frac{1}{2} \text{tr}(\boldsymbol{\Sigma} d\boldsymbol{\Sigma}^{-1} \boldsymbol{\Sigma} d\boldsymbol{\Sigma}^{-1}). \quad (107)$$

The expected value of the second differential over q is

$$\begin{aligned} -\mathbb{E}_q [d^2 \ln q] &= d\boldsymbol{\mu}^T \boldsymbol{\Sigma}^{-1} d\boldsymbol{\mu} + \frac{1}{2} \text{tr}(\boldsymbol{\Sigma} d\boldsymbol{\Sigma}^{-1} \boldsymbol{\Sigma} d\boldsymbol{\Sigma}^{-1}) \\ &= d\boldsymbol{\mu}^T \boldsymbol{\Sigma}^{-1} d\boldsymbol{\mu} + \frac{1}{2} \text{vec}(d\boldsymbol{\Sigma}^{-1})^T (\boldsymbol{\Sigma} \otimes \boldsymbol{\Sigma}) \text{vec}(d\boldsymbol{\Sigma}^{-1}). \end{aligned} \quad (108)$$

In matrix form this is

$$-\mathbb{E}_q [d^2 \ln q] = d\boldsymbol{\alpha}^T \begin{bmatrix} \boldsymbol{\Sigma}^{-1} & \mathbf{0} \\ \mathbf{0} & \frac{1}{2}(\boldsymbol{\Sigma} \otimes \boldsymbol{\Sigma}) \end{bmatrix} d\boldsymbol{\alpha}, \quad (109)$$

where

$$d\boldsymbol{\alpha} = \begin{bmatrix} d\boldsymbol{\mu} \\ \text{vec}(d\boldsymbol{\Sigma}^{-1}) \end{bmatrix}. \quad (110)$$

Turning the differentials into partial derivatives we have

$$\mathcal{I}_\alpha = -\mathbb{E}_q \left[\frac{\partial^2 \ln q}{\partial \alpha^T \partial \alpha} \right] = \begin{bmatrix} \boldsymbol{\Sigma}^{-1} & \mathbf{0} \\ \mathbf{0} & \frac{1}{2}(\boldsymbol{\Sigma} \otimes \boldsymbol{\Sigma}) \end{bmatrix}. \quad (111)$$

The inverse FIM is given by

$$\mathcal{I}_\alpha^{-1} = \begin{bmatrix} \mathcal{I}_\mu^{-1} & \mathbf{0} \\ \mathbf{0} & \mathcal{I}_{\boldsymbol{\Sigma}^{-1}}^{-1} \end{bmatrix} = \begin{bmatrix} \boldsymbol{\Sigma} & \mathbf{0} \\ \mathbf{0} & 2(\boldsymbol{\Sigma}^{-1} \otimes \boldsymbol{\Sigma}^{-1}) \end{bmatrix}, \quad (112)$$

using properties of linear and Kronecker algebra.

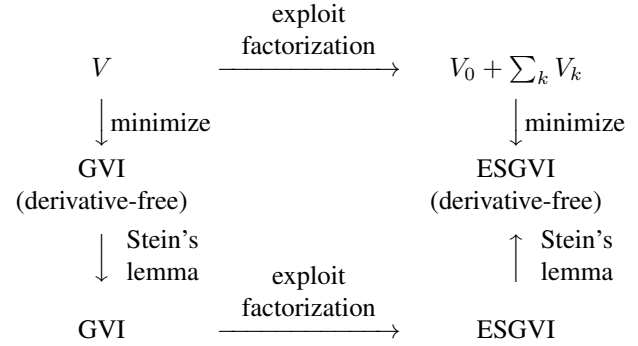


Figure 11. Commutative diagram showing two paths to get to the derivative-free version of ESGVI starting from the loss functional, V .

C Direct Derivation of Derivative-Free ESGVI

In our main ESGVI derivation, we chose to (i) define a scheme to minimize $V(q)$ with respect to q and then (ii) exploit $\phi(\mathbf{x}) = \sum_{k=1}^K \phi_k(\mathbf{x}_k)$ to make the scheme efficient. Here we show that we can carry out (i) and (ii) in the opposite order to streamline the derivation of the derivative-free version of ESGVI, avoiding the need for Stein's lemma.

Figure 11 shows two paths to get to the derivative-free version of ESGVI starting from our loss functional, V . The main body of the paper took the counter-clockwise path that goes down, across to the right, and then up. We will now demonstrate the clockwise path that goes right and then down.

Inserting $\phi(\mathbf{x}) = \sum_{k=1}^K \phi_k(\mathbf{x}_k)$, the loss functional becomes

$$V(q) = \sum_{k=1}^K \underbrace{\mathbb{E}_{q_k}[\phi_k(\mathbf{x}_k)]}_{V_k(q_k)} + \underbrace{\frac{1}{2} \ln(|\boldsymbol{\Sigma}^{-1}|)}_{V_0}, \quad (113)$$

where the expectations are now over the marginal, $q_k(\mathbf{x}_k) = \mathcal{N}(\boldsymbol{\mu}_k, \boldsymbol{\Sigma}_{kk})$ with

$$\boldsymbol{\mu}_k = \mathbf{P}_k \boldsymbol{\mu}, \quad \boldsymbol{\Sigma}_{kk} = \mathbf{P}_k \boldsymbol{\Sigma} \mathbf{P}_k^T, \quad (114)$$

and where \mathbf{P}_k is a projection matrix. We then take the first derivative with respect to $\boldsymbol{\mu}$:

$$\begin{aligned} \frac{\partial V(q)}{\partial \boldsymbol{\mu}^T} &= \frac{\partial}{\partial \boldsymbol{\mu}^T} \left(\sum_{k=1}^K \mathbb{E}_{q_k}[\phi_k(\mathbf{x}_k)] + \frac{1}{2} \ln(|\boldsymbol{\Sigma}^{-1}|) \right) \\ &= \sum_{k=1}^K \frac{\partial}{\partial \boldsymbol{\mu}^T} \mathbb{E}_{q_k}[\phi_k(\mathbf{x}_k)] \\ &= \sum_{k=1}^K \mathbf{P}_k^T \frac{\partial}{\partial \boldsymbol{\mu}_k^T} \mathbb{E}_{q_k}[\phi_k(\mathbf{x}_k)] \\ &= \sum_{k=1}^K \mathbf{P}_k^T \boldsymbol{\Sigma}_{kk}^{-1} \underbrace{\mathbb{E}_{q_k}[(\mathbf{x}_k - \boldsymbol{\mu}_k) \phi_k(\mathbf{x}_k)]}_{\text{cubature}}. \end{aligned} \quad (115)$$

The last step comes from (10a) applied at the marginal level. Similarly, we have for the second derivative with respect to $\boldsymbol{\mu}$ that

$$\begin{aligned}
 & \frac{\partial^2 V(q)}{\partial \boldsymbol{\mu}^T \partial \boldsymbol{\mu}} \\
 &= \frac{\partial^2}{\partial \boldsymbol{\mu}^T \partial \boldsymbol{\mu}} \left(\sum_{k=1}^K \mathbb{E}_{q_k} [\phi_k(\mathbf{x}_k)] + \frac{1}{2} \ln(|\boldsymbol{\Sigma}^{-1}|) \right) \\
 &= \sum_{k=1}^K \frac{\partial^2}{\partial \boldsymbol{\mu}^T \partial \boldsymbol{\mu}} \mathbb{E}_{q_k} [\phi_k(\mathbf{x}_k)] \\
 &= \sum_{k=1}^K \mathbf{P}_k^T \left(\frac{\partial^2}{\partial \boldsymbol{\mu}_k^T \partial \boldsymbol{\mu}_k} \mathbb{E}_{q_k} [\phi_k(\mathbf{x}_k)] \right) \mathbf{P}_k \\
 &= \sum_{k=1}^K \mathbf{P}_k^T \left(\underbrace{\boldsymbol{\Sigma}_{kk}^{-1} \mathbb{E}_{q_k} [(\mathbf{x}_k - \boldsymbol{\mu}_k)(\mathbf{x}_k - \boldsymbol{\mu}_k)^T \phi_k(\mathbf{x}_k)]}_{\text{cubature}} \right. \\
 &\quad \left. \times \boldsymbol{\Sigma}_{kk}^{-1} - \underbrace{\boldsymbol{\Sigma}_{kk}^{-1} \mathbb{E}_{q_k} [\phi_k(\mathbf{x}_k)]}_{\text{cubature}} \right) \mathbf{P}_k, \quad (116)
 \end{aligned}$$

where we made use of (10b) at the marginal level in the last step.

The update scheme is then

$$(\boldsymbol{\Sigma}^{-1})^{(i+1)} = \frac{\partial^2 V(q)}{\partial \boldsymbol{\mu}^T \partial \boldsymbol{\mu}} \Big|_{q^{(i)}}, \quad (117a)$$

$$(\boldsymbol{\Sigma}^{-1})^{(i+1)} \delta \boldsymbol{\mu} = - \frac{\partial V(q)}{\partial \boldsymbol{\mu}^T} \Big|_{q^{(i)}}, \quad (117b)$$

$$\boldsymbol{\mu}^{(i+1)} = \boldsymbol{\mu}^{(i)} + \delta \boldsymbol{\mu}, \quad (117c)$$

which is identical to the derivative-free ESGVI approach from the main body of the paper. The sparsity of the left-hand side comes from the use of the projection matrices. We did not require the use of Stein's lemma (Stein 1981) using this derivation, which also means that we have made no assumptions about the differentiability of $\phi_k(\mathbf{x}_k)$ with respect to \mathbf{x}_k . A similar streamlined derivation can be worked out for the Gauss-Newton variant.

D Derivation of Derivative Identities (24)

To show (24a), we can use (10a) to write

$$\frac{\partial}{\partial \boldsymbol{\mu}^T} \mathbb{E}_q[f(\mathbf{x})] = \boldsymbol{\Sigma}^{-1} \mathbb{E}_q[(\mathbf{x} - \boldsymbol{\mu})f(\mathbf{x})], \quad (118)$$

which can also be found in Oppier and Archambeau (2009). Applying Stein's lemma from (22) we immediately have

$$\frac{\partial}{\partial \boldsymbol{\mu}^T} \mathbb{E}_q[f(\mathbf{x})] = \mathbb{E}_q \left[\frac{\partial f(\mathbf{x})}{\partial \mathbf{x}^T} \right], \quad (119)$$

the desired result.

To show (24b), we can use (10b) to write

$$\begin{aligned}
 \frac{\partial^2}{\partial \boldsymbol{\mu}^T \partial \boldsymbol{\mu}} \mathbb{E}_q[f(\mathbf{x})] &= \boldsymbol{\Sigma}^{-1} \mathbb{E}_q[(\mathbf{x} - \boldsymbol{\mu})(\mathbf{x} - \boldsymbol{\mu})^T f(\mathbf{x})] \boldsymbol{\Sigma}^{-1} \\
 &\quad - \boldsymbol{\Sigma}^{-1} \mathbb{E}_q[f(\mathbf{x})], \quad (120)
 \end{aligned}$$

again due to Oppier and Archambeau (2009). Applying Stein's lemma from (23) we have

$$\frac{\partial^2}{\partial \boldsymbol{\mu}^T \partial \boldsymbol{\mu}} \mathbb{E}_q[f(\mathbf{x})] = \mathbb{E}_q \left[\frac{\partial^2 f(\mathbf{x})}{\partial \mathbf{x}^T \partial \mathbf{x}} \right], \quad (121)$$

the desired result. Similarly to (10c), we have

$$\begin{aligned}
 \frac{\partial}{\partial \boldsymbol{\Sigma}^{-1}} \mathbb{E}_q[f(\mathbf{x})] &= -\frac{1}{2} \mathbb{E}_q[(\mathbf{x} - \boldsymbol{\mu})(\mathbf{x} - \boldsymbol{\mu})^T f(\mathbf{x})] \\
 &\quad + \frac{1}{2} \boldsymbol{\Sigma} \mathbb{E}_q[f(\mathbf{x})], \quad (122)
 \end{aligned}$$

which is again confirmed by Oppier and Archambeau (2009). Comparing the right-hand side of this to the right-hand side of (120), we have

$$\begin{aligned}
 -2\boldsymbol{\Sigma}^{-1} \left(\frac{\partial}{\partial \boldsymbol{\Sigma}^{-1}} \mathbb{E}_q[f(\mathbf{x})] \right) \boldsymbol{\Sigma}^{-1} &= \frac{\partial^2}{\partial \boldsymbol{\mu}^T \partial \boldsymbol{\mu}} \mathbb{E}_q[f(\mathbf{x})] \\
 &= \mathbb{E}_q \left[\frac{\partial^2 f(\mathbf{x})}{\partial \mathbf{x}^T \partial \mathbf{x}} \right], \quad (123)
 \end{aligned}$$

which shows the second part of (24b).